LEVEL II

12

WRC-R-308

AD A105896

DARPA ORDER NUMBER: 3747, Amendment 3

CONTRACTOR: WESTERN RESEARCH CORPORATION
8616 Commerce Avenue
San Diego, California 92121

TITLE: Final Technical Report:
The Transverse Rf Accelerator

PROJECT ENGINEER: Nino R. Pereira
(714) 578-5885

EFFECTIVE DATE OF CONTRACT: 15 August 1980

CONTRACT EXPIRATION DATE: 15 February 1981

SPONSORED BY: DEFENSE ADVANCED RESEARCH PROJECTS AGENCY (DoD), DARPA Order No. 3747, Amendment 3

Monitored by ONR
under Contract No. N00014-80-C-0902

NOTICE OF DISCLAIMER: The views and conclusions contained in this document are those of the authors and should not be interpreted as necessarily representing the official policies, either expressed or implied, of the Defense Advanced Research Projects Agency; or the U. S Government.

DTIC FILE COPY

DTIC ELECTE OCT 21 1981 S D

DATE OF REPORT: 11 September 1981

DISTRIBUTION STATEMENT A
Approved for public release;
Distribution Unlimited

81 9 28 007

(14) WRC-R-308

DARPA ORDER NUMBER: 3747, Amendment 3

CONTRACTOR: WESTERN RESEARCH CORPORATION
8616 Commerce Avenue
San Diego, CA 92121

(15)

CONTRACT NUMBER (9) N00014-80-C-0902, // DARPA Order-3747

TITLE: (6) Final Technical Report: 15 Aug 80-15 Feb 81,
The Transverse Rf Accelerator.

PROJECT ENGINEER: (10) Nino R. Pereira
(714) 578-5885

EFFECTIVE DATE OF CONTRACT: 15 August 1980

CONTRACT EXPIRATION DATE: 15 February 1981

SPONSORED BY: DEFENSE ADVANCED RESEARCH PROJECTS AGENCY (DoD)
DARPA Order Number 3747, Amendment 3

Monitored by ONR under Contract N00014-80-C-0902

NOTICE OF DISCLAIMER: The views and conclusions contained in this document are those of the authors and should not be interpreted as necessarily representing the official policies, either expressed or implied, of the Defense Advanced Research Projects Agency; or the U. S. Government.

DATE OF REPORT: (11) 11 September 1981 (12) 93

Accession For	
NTIS GRA&I	X
DTIC TAB	☐
Unannounced	☐
Justification	
By Per Ltr. on file	
Distribution/	
Availability Codes	
Dist	Avail and/or Special
A	

DTIC ELECTE OCT 21 1981 S D

D

395516 (B)

DISTRIBUTION STATEMENT A
Approved for public release;
Distribution Unlimited

CONTENTS

FIGURES

SECTION I

REPORT SUMMARY

High electric fields are obviously advantageous in powerful electron accelerators: for a given energy gain per particle, the device length is inversely proportional to the maximum field; and the maximum current is roughly proportional to the field. The transverse RF accelerator provides a high field strength by using an accelerator cavity analogous to an optical resonator: the focussing of electromagnetic energy produces large fields along the cavity axis for manageable fields at the wall. In addition, it is possible to have the fields largely transverse, permitting very high accelerating gradients. This report discusses two basic topics: the field structure as related to the acceleration mechanism, and limitations on the electric field strength. Important aspects that are not part of the research objectives are the accelerator power requirements, the effects of cavity loading, and other phenomena.

The accelerator cavity can be conceptually generated from a linear optical resonator as shown in Figure 1a. The resonator is then rotated about an axis in the focal plane, to give the cylindrical resonator of Figure 1b. This configuration gives large intensities in the shaded region, from the combined effect of axial focussing already present in Figure 1a, and the radial focussing introduced by the rotation. Finally, the accelerator cavity, in Figure 1c, is extended axially to allow wavelengths comparable to cavity dimensions.

The electromagnetic cavity modes suitable for electron acceleration have a purely azimuthal magnetic field, and an mostly axial electric field. The modes can be found exactly. However, in the interesting parameter region the modes are close to the well-known higher order Hermite-Gaussian optical resonator modes shown in Figure 2a. The electric field direction during one half-cycle is as given in Figure 2b, and is reversed in the other half-cycle. The field is obviously cylindrically symmetric, and extends out to the cavity wall.

The accelerator process is illustrated in Figure 3. As an electron enters the first lobe in the spatial field pattern, Figure 3a , the field points opposite to the electron velocity, and the negatively charged electron increases its momentum (but not its velocity) during the first half-cycle of the field $o<\omega t<\pi$. At $\omega t = \pi$ the field reverses, and the situation is as given in Figure 3b: at this time the electron shown has not yet left the first spatial lobe, and it loses momentum. Again, the electron's velocity remains constant, so that a short time ϵ/ω later the electron enters the middle lobe, (Figure 3c), where it is again accelerated until it leaves this lobe or ωt reaches 2π , whichever is first. At this point there might be another momentum decrease, but it is obvious that the net effect of the various accelerations and decelerations is a net energy gain ΔE of order $\Delta E \simeq eE_p L/2$, where E_p is a typical field strength, and L is the width of the spatial pattern as indicated in Figure 3c. From the discussion it is clear that the acceleration process is, basically, resonant wave-particle interaction with an approximately sinusoidal wave. The calculated energy transfer is shown in Figure 4.

The accelerating field strength is intrinsically limited by the allowable field at the cavity wall. The normal field component will be limited by electric breakdown to 30 MeV/m or so, but the parallel

component should be up to the skin current heating limit of $\simeq 10^9$ V/m (the estimate is justified in Appendix I). Therefore it is necessary to know the direction of the field at the wall, and to select a cavity geometry or accelerator operating regime where the electric field is mainly parallel to the wall. A simple argument for the field direction gives $E_\perp/E_\parallel \simeq \lambda/\ell_\parallel$, where $\lambda = \omega/c$ is the free space wavelength and $\ell_\parallel$ is a typical length scale of the field pattern on the wall (see Appendix II).

The above estimate indicates that the large wall fields predicted for the transverse RF accelerator are obtainable when the free-space wavelength is small compared to the wavelength of the fields on the wall. This is assured if the cavity is used with a high mode number in the radial direction, or a high frequency. An approximate formula is given in Appendix III.

The transverse accelerator research reported on here concentrated on these topics. To summarize:

i) use of laser-like higher order cavity modes in approximate resonance with relativistic electrons, and
ii) the ability to make the electric fields at the wall largely transverse, leading to very high field gradients, and
iii) accelerating electric fields in the center that are enhanced by radial focussing.

The qualitative description given above is substantiated by the analyses in the appendices. Here we give briefly their conclusions.

Appendix I derives the limit to the parallel electric field $E_{\parallel} \simeq 10^9$ V/m , by balancing the Joule heating due to skin currents with the conductive heat transfer into the cavity walls.

The exact expressions for the accelerator cavity modes are given in Appendix II. The modes consist of a single magnetic field component, $B_\phi (r,z)$, which is a product of the axial and spheroidal wave function. The electric field has an axial and radial component given by the curl of B_ϕ (times $c^2/i\omega$) . Exact expressions can then be written down for the quantities of interest, e.g. $E_{\perp,wall}/E_{\parallel,axis}$, the cavity loading, the total energy in the cavity, etc.

The other appendices work out some of the details in the formulation, and/or contain numerical evaluations. Appendix III gives the field ratio $E_\perp/E_\parallel$ in terms of axial mode number, and cavity frequency and shape.

Appendix IV derives the electron acceleration, and does the emittance calculation. Here the fields are approximated by their Gaussian-Hermite form. The energy gain is again a Gaussian-Hermite function of the frequency $\omega^{\frac{1}{2}}$. The transverse momentum transfer on axis vanishes by symmetry, but the maximum transverse momentum gain, at about $\lambda/4$ off-axis, is of the same order as the parallel gain: therefore the radial bunch width should be small compared to a wavelenth.

Finally, Appendix V is a compendium of mathematical formulae that were found useful in the course of the analysis. One item may be interesting, namely a numerical comparison of the spheroidal functions with the various approximations used throughout. Appendix VI is a collection of miscellaneous physics results, and Appendix VII treats open cavities.

The overall conclusion from these analyses, and especially from numerical evaluations at MRC in Appendix VIII (AMRC-N-156) is that the transverse RF accelerator's performance is limited by the ratio

$$\Delta E/eE_{\perp} \; L \lesssim 0.5 - 1.0 \quad . \tag{1}$$

Here ΔE is the energy transfer to the electrons, L the cavity length, and $E_{\perp}$ a typical normal wall field. This value is comparable to that obtained in conventional cavities, and there appears to be no advantage in using cavities generated by extending optical resonators to the microwave regime.

Although we know of no fundamental limitations indicating that Equation (1) is a fundamental limit for all cavities, possibly with some factor of order unity, it appears for the moment that the decisive way to improve the accelerating gradient is to increase the breakdown limit to $E_{\perp}$.

No detailed analysis has yet been made for purely propagating modes that are geometrically focussed down to a small focal region. This way one has a handle on the spatial field pattern on the wall, through the placement of the emitters on the wall. Therefore, the field direction, $E_{\perp}/E_{\parallel}$, (with $E_{\parallel}$ at $\lambda/4$ away from the wall) is under control.

Using a forced mode instead of a cavity eigenmode allows one to select a frequency relatively independent from the field pattern on the wall. Therefore, the coupling to the particles can be somewhat influenced because the coupling partially determined by the field frequency.

If the search for a large coupling together with small normal wall fields continues to give negative results, we must conclude that the desired increase in accelerating gradient should be sought elsewhere, for example by increasing the breakdown limit by more suitable wall materials, or local magnetic insulation.

ORIGIN OF RESONATOR CAVITY

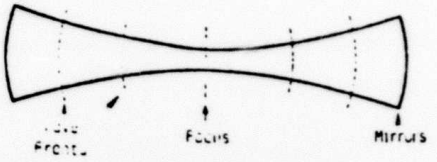

a. Linear Optical Resonator

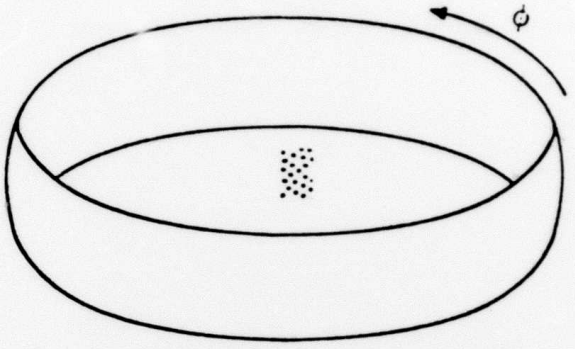

b. Cylindrically Symmetric Resonator

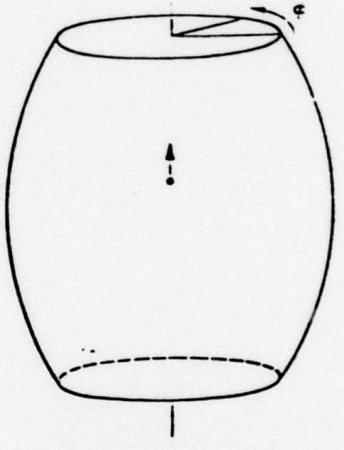

c. Accelerator Cavity

FIGURE 1

From A. E. Siegman "An Introduction to Lasers and Masers"

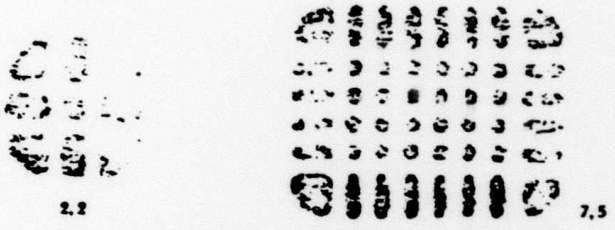

FIG. 8-23 Examples of higher-order Hermite gaussian optical-resonator modes as photographed in the output beam of a laser oscillator.

(linear)

Figure 2a.

Figure 2 Field directions in cavity mode (2,2) during one half-cycle.

FIGURE 2

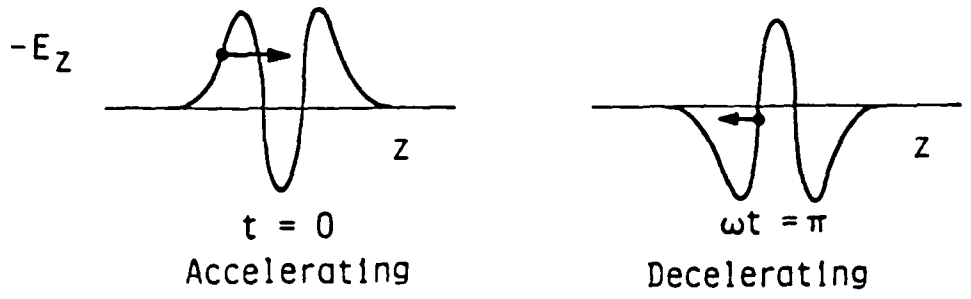

t = 0
Accelerating

a.

$\omega t = \pi$
Decelerating

b.

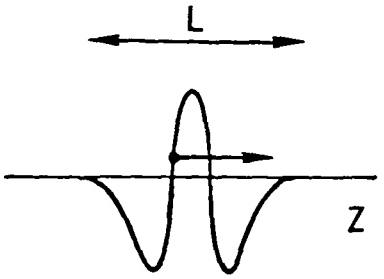

$\omega t = \pi + \epsilon$
Accelerating

c.

Figure 3.

1.

$$\frac{\Delta E}{eE_p'\lambda}$$

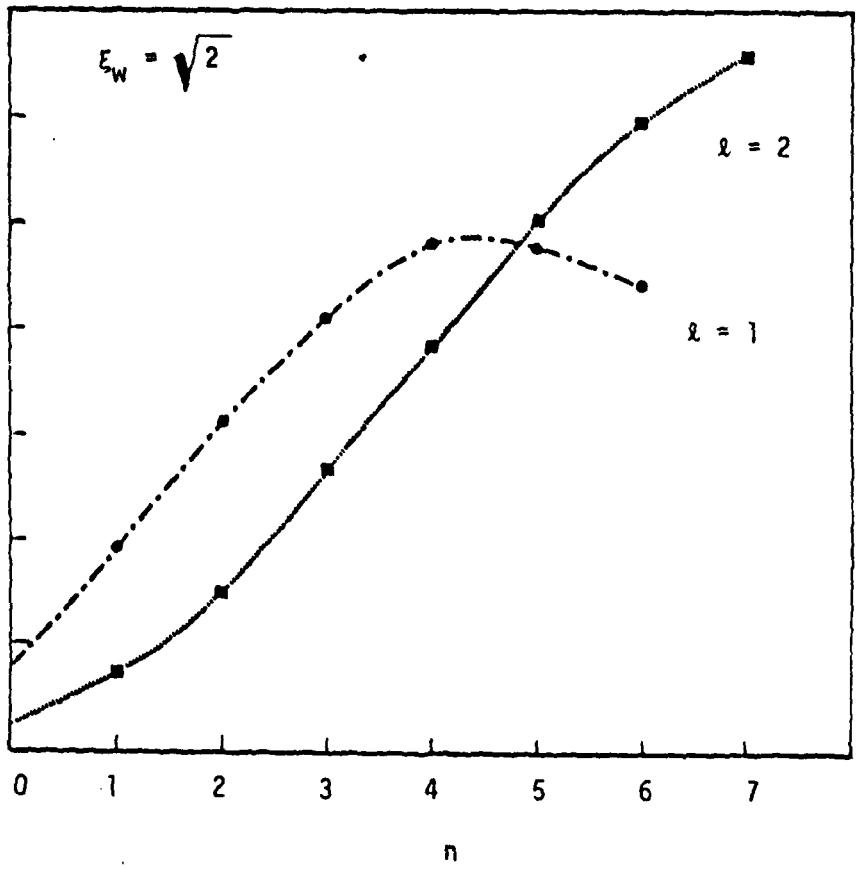

Figure 4. Energy gain as function of axial mode number n for radial mode numbers ℓ = 1 and ℓ =2, in a confocal resonator.

APPENDIX I

TRANSVERSE RF PEAK FIELD STRENGTH ESTIMATES

The peak electric field strength $E_\perp$ normal to a conducting surface is typically on the order of 10^7 volts per meter. This value is set by breakdown due to electron emission and/or particle bombardment. Larger $E_\perp$'s are possible, for example, by magnetically insulating the conducting surface in the high gradient region with a parallel magnetic field perpendicular to the electric field. The accelerating gradient of particle accelerators using normal fields is comparable to $eE_\perp\lambda$: any technology that increases the attainable $E_\perp$'s could have an impact on the maximum acceleration.

However, it is also possible to produce an accelerator with high magnetic fields strengths $B_\parallel$ parallel to the wall, and negligible normal electric field components. This may be accomplished by utilizing mirrors to reflect a travelling wave, as is common practice in laser work. The wave direction is normal to the wall, and the magnetic field (and the accompanying electric field) is perpendicular to the propagation direction.

Normal reflection from a good conductor results in a very small electric field at the surface, since the reflected wave interferes destructively with the incoming wave at the conducting surface. The failure mechanism for such a surface is different from that of electric breakdown. For the regime of interest, failure is due to the surface layer heating by the currents induced by the incoming wave. This is known as the skin depth effect, since the electric and magnetic fields only penetrate approximately one skin depth. This failure mechanism scales with

frequency and conductivity of the reflector; it also depends on the heat transfer rate from the skin depth layer to the interior.

The reflecting power for normal incidence on a plane conducting surface is $R = 1 - S$; Here S is, approximately,

$$S \simeq \sqrt{\frac{16\pi\ \varepsilon_o \nu}{\sigma}}$$

where ν is the frequency (in Hz) and σ the electrical conductivity (in $(\Omega m)^{-1}$). The energy per surface area absorbed in the conductor is equal to S, times the average electric density $\frac{1}{4}\epsilon_o |E_p|^2$ (E_p is the peak field strength, in V/m), and the pulse length τ_p times the light speed c.

The conductivity of copper is function of temperature is shown in Figure 1. The conductivity changes one order of magnitude from room temperature $T \simeq 300°K$ to the melting point at about $1000°K$. A reasonable average value over this temperature range is $\sigma \simeq 3 \times 10^7\ (\Omega m)^{-1}$. The conductivity could be increased by an order of magnitude when the mirrors are cold, $10°K$ say, at the beginning of the electric field buildup.

The energy is deposited as heat over one electrical skin depth,

$$\delta_e = \sqrt{\frac{2}{\mu\sigma\omega}}\ :$$

the heat diffuses inward over a characteristic distance

$$\delta_{th} \simeq \sqrt{\Lambda\tau_p / \pi c_v}\ .$$

where Λ is the thermal conductivity, and c_v is the heat capacity at constant volume. For copper at room temperature the thermal conductivity is

$\Lambda \approx 400$ $(Jm^{-1}sec^{-1}{}^{\circ}K^{-1})$, the heat capacity $c_v \approx 3.5 \times 10^6$ $(Jm^{-3}\,{}^{\circ}K^{-1})$. For oscillating heat load a "thermal skin depth" can be defined in analogy to the electrical skin depth. Setting $\omega = 2\pi/\tau_p$,

$$\delta_e/\delta_{th} \approx \sqrt{\frac{c_v}{\sigma\mu\Lambda}} :$$

the numerical value for copper at room temperature is about 10.

Since the thermal skin depth is an order of magnitude smaller than the electrical skin depth, there will be little influence from heat diffusion over a typical oscillation timescale $\tau \approx 2\pi/\omega$. After about 100 oscillations, however, the heat conduction starts to come in, and for even longer times the heat conduction dominates. The frequency and pulse width envisioned for the RF cavity is about 1GHz and $\tau_p \approx 10^{-6}$ sec, or about 1000 oscillations. Hence it is marginally reasonable to assume that heat conduction can spread the heat over the thermal diffusion length $\delta_{th} \approx \sqrt{\Lambda/\pi c_v}\,\tau_p^{\frac{1}{2}}$.

Mirror failure is defined by the melting of the reflector. This occurs when the input energy has increased the mirror temperature to the melting point, about $10^3{}^{\circ}K$ for copper. Therefore, the peak field is limited by

$$\frac{1}{4}\,\varepsilon_o\,|E_p|^2\,c\tau_p\sqrt{\frac{16\pi\varepsilon_o}{\sigma}}\;\nu^{\frac{1}{2}} \approx c_v\,\Delta T\sqrt{\frac{\Lambda}{\pi c_v}}\,\tau_p^{\frac{1}{2}}\ ,$$

where ΔT is the temperature increase. Inserting the numerical values leads to

$$E_p \approx 3 \times 10^9\,(\tau_p\nu)^{-\frac{1}{4}}\ (V/m)\ .$$

Some limitations of the above analysis are obvious: the neglect of the spatial dependence exp - $2x/\delta_e$ in the heat generation, the assumption

that the heat is spread out evenly over a thermal diffusion length, and the decrease of conductivity with increasing temperature all tend to increase the peak field estimate. The assumption that the peak field is attained instantaneously instead of increasing linearly with time decreases the estimate. A working estimate for our purposes will be

$$E_p \approx 10^9 (\tau_p \nu)^{-\frac{1}{4}} \text{ V/m} \quad .$$

Data from laser mirror failure tend to corroborate the above estimate.

A more complete analysis would use the heat diffusion equation

$$c_v \frac{\partial T}{\partial t} = \frac{j_o^2}{2\sigma(T)} \exp - 2x/\delta_e(T) + \Lambda(T) \frac{\partial^2 T}{\partial x^2} \quad :$$

analytic solution of this equation is not possible except under simplifying assumptions[3] (σ constant, etc) similar to the ones made above.

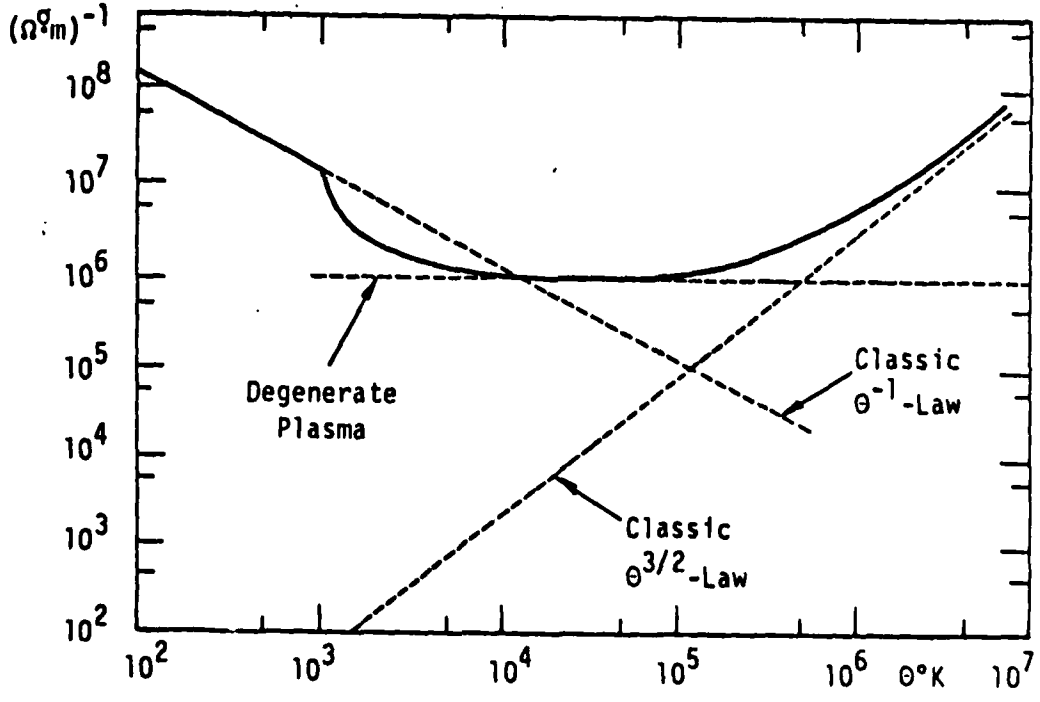

Figure 1. Approximate behavior of electrical conductivity for copper as a function of temperature (From Ref. 2).

REFERENCES

1. See eg. W. K. H. Panofski and M. Phillips, "Classical Electricity and Magnetism, 2nd Ed.", Addison-Wesley, 1964, Eq. 11-63.

2. H. Knoepfel, "Pulsed High Magnetic Fields," North Holland, 1970, Fig. 10.23.

3. Ref. 2, Section 4.20.

APPENDIX II

ELECTROMAGNETIC FIELDS IN ELLIPSOIDAL CAVITY

The electromagnetic fields envisioned in the transverse RF accelerator have the electric vector mainly parallel to the cavity axis, while the magnetic field is roughly perpendicular to the axis. These conditions are satisfied by one case that is exactly solvable, namely the purely solenoidal oscillations mentioned by Meixner, (Reference 1, Sections 4.41 and 4.43). The particular case where all fields can be derived from one magnetic field component B_ϕ (see Figure 1) will now be discussed.

Maxwell's equations in vacuum are

$$\nabla \times \underline{E} = - \frac{\partial \underline{B}}{\partial t} \quad , \tag{1a}$$

$$\nabla \times \underline{B} = \mu_o \underline{j} + \frac{1}{c^2} \frac{\partial \underline{E}}{\partial t} \quad ; \tag{1b}$$

here $\underline{j}$ is the current density, and all quantities are in MKS units. It is simpler to work with a system where various factors c are absorbed: defining.

$$\underline{B}' = c\underline{B} \ , \ \underline{J} = \mu_o c \underline{j} \ , \tag{2}$$

and dropping the primes, equation (1) becomes

$$\nabla \times \underline{E} = - \frac{1}{c} \frac{\partial \underline{B}}{\partial t} \quad , \tag{3a}$$

$$\nabla \times \underline{B} = \underline{J} + \frac{1}{c} \frac{\partial \underline{E}}{\partial t} \quad . \tag{3b}$$

These equations can be combined into

$$\nabla \times \nabla \times \underline{B} = \nabla \times \underline{J} - \frac{1}{c^2} \frac{\partial^2 \underline{B}}{\partial t^2} \quad . \tag{4}$$

The free oscillations of the ellipsoidal resonator are obtained by setting $\underline{J} = 0$ and assuming a harmonic time dependence exp - iωt.

$$\nabla \times \nabla \times \underline{B} = k^2 \underline{B} \quad , \tag{5}$$

with $k = \omega/c$, and with the boundary condition that the electric field parallel to the cavity wall be zero.

In an arbitrary orthogonal curvilinear coordinate system, equation (5) for the B_3 component of the magnetic field becomes:

$$h_1 h_2 k^2 B_3 + \frac{\partial}{\partial q_1} \frac{h_2}{h_3 h_1} \frac{\partial}{\partial q_1} h_3 B_3 + \frac{\partial}{\partial q_2} \frac{h_1}{h_2 h_3} \frac{\partial}{\partial q_2} h_3 B_3 = 0. \tag{6}$$

For prolate ellipsoidal coordinates (see Figure 2), where

$$\begin{aligned} & q_1 = \eta, \quad q_2 = \xi, \quad q_3 = \phi \quad ; \\ & x = r \cos \psi, \quad y = r \sin \psi \quad , \\ & r = \frac{f}{2} (1-\eta^2)^{\frac{1}{2}} (\xi^2-1)^{\frac{1}{2}} \quad , \\ & z = \frac{f}{2} \eta \xi \quad , \end{aligned} \tag{7}$$

where f is the focal distance, the coordinates and scale factors are

$$\begin{aligned} & h_1 = \frac{f}{2} (\xi^2-\eta^2)^{\frac{1}{2}} / (\xi^2-1)^{\frac{1}{2}} \quad ; \\ & h_2 = \frac{f}{2} (\xi^2-\eta^2)^{\frac{1}{2}} / (1-\eta^2)^{\frac{1}{2}} \quad , \\ & h_3 = \frac{f}{2} (1-\eta^2)^{\frac{1}{2}} (\xi^2-1)^{\frac{1}{2}} \quad . \end{aligned} \tag{8}$$

Then equation (6) becomes

$$\left(\frac{kf}{2}\right)^2 (\xi^2-\eta^2)\, B_3 + (1-\eta^2)^{\frac{1}{2}} \frac{\partial^2}{\partial\eta^2} (1-\eta^2)^{\frac{1}{2}} B_3 + (\xi^2-1)^{\frac{1}{2}} \frac{\partial^2}{\partial\xi^2} (\xi^2-1)^{\frac{1}{2}} B_3 = 0, \quad (9)$$

which is clearly separable, but a non-standard form of the spheroidal equation. With the relation (equation for ξ)

$$\left[(\xi^2-1)^{\frac{1}{2}} \frac{\partial^2}{\partial\xi^2} (\xi^2-1)^{\frac{1}{2}}\right] B_3 = \left[\frac{\partial}{\partial\xi} (\xi^2-1) \frac{\partial}{\partial\xi} - \frac{1}{\xi^2-1}\right] B_3 \quad , \quad (10)$$

one obtains the spheroidal wave equation for $m=1$:

$$\left[\frac{\partial}{\partial\xi} (\xi^2-1) \frac{\partial}{\partial\xi} + \frac{\partial}{\partial\eta} (1-\eta^2) \frac{\partial}{\partial\eta} + (\xi^2-\eta^2)\left(\frac{kf}{2}\right)^2 - \frac{1}{\xi^2-1} - \frac{1}{1-\eta^2}\right] B_3 = 0. \quad (11)$$

Hence the exact solution is given as a product of two spheroidal wave functions and their derivatives:

$$B_\phi(\xi,\eta) = \text{const.}\ R_{1n}(h,\xi)\ S_{1n}(h,\eta) \quad , \quad (12)$$

where h is the parameter

$$h = \frac{kf}{2} \quad . \quad (13)$$

The electric field component parallel to the cavity wall $\xi = \xi_o = \text{constant}$, is E_η :

$$E_\eta = -\frac{i}{h} \sqrt{\frac{1}{\xi^2-\eta^2}} \frac{\partial}{\partial\xi} \sqrt{\xi^2-1}\, B_\phi \quad ; \quad (14)$$

the boundary condition is that $E_\eta = 0$, hence a somewhat complicated condition on the zeroes of the first derivative of the radial spheriodal function, as will be seen below. Numerical work appears to be necessary for firm results. The normal electric field is

$$E_\xi = \frac{i}{h}\sqrt{\frac{1}{\xi^2-\eta^2}}\ \frac{\partial}{\partial\eta}\sqrt{1-\eta^2}\ B_\phi \quad . \tag{15}$$

These formulas give the exact fields in an ellipsoidal cavity.

An attractive feature in the transverse RF accelerator is the reduction of normal electric field at the wall $\xi = \xi_o$ compared to the maximum field strength that accelerates the particles along the z-axis at $\xi = 1$. Therefore one should evaluate the maximum

$$\frac{E_\xi\big|_{\xi=\xi_o}}{E_\eta\big|_{\substack{\xi=1\\ \max.\eta}}} = \frac{R_{1n}(h,\xi_o)\left\{(\xi_o^2-\eta^2)^{-\frac{1}{2}}\frac{\partial}{\partial\eta}\left[(1-\eta^2)^{\frac{1}{2}}S_{1n}(h,\eta)\right]\right\}_{\max}}{\left\{(1-\eta^2)^{-\frac{1}{2}}S_{1n}(h,\eta)\right\}_{\max}\ \frac{\partial}{\partial\xi}\left[\sqrt{\xi^2-1}\ R_{1n}(h,\xi)\right]_{\xi=1_o}}, \tag{16}$$

in addition to the energy transfer to accelerated particles given, essentially, by the Fourier transform of equation 14.

Before continuing with the exact formulas (14)-(16), a few remarks are in order.

i. The derivation of equation 11 is not elegant: another derivation is as follows. Consider the relation (problem 13.7 of Reference 6)

$$-\nabla\times\nabla\times\left[\underline{e}_\phi\,\psi\right] = \underline{e}_\phi\left[\nabla^2\psi - \frac{\psi}{r^2}\right] \quad , \tag{17}$$

where $\underline{e}_\phi$ is the unit vector in the azimuthal direction, and $\psi=4(r,z)$ is rotationally symmetric. (This relation is easily verified in cylindrical coordinates). The $-\psi/r^2$ term can be conceptually generated from the azimuthal mode $\psi\cos\phi$ $(m=1)$ in the Laplacian. Hence equation (11) follows directly.

ii. The functions $U_n(\eta) = (1-\eta^2)^{\frac{1}{2}} S_{1n}(h,\eta)$ and $V_n(\xi) = (\xi^2-1)^{\frac{1}{2}} R_{1n}(h,\xi)$ are entire functions: in particular near $\xi,\eta = 1$ there are no singularities. For numerical purposes it may be nicer to integrate the differential equations for U_n and V_n in a search for the correct boundard condition $E_\eta = 0$. The appropriate equation is a separated version of equation 9.

$$(1-\eta^2)\frac{\partial^2 U_n}{\partial \eta^2} + (\lambda^2 - h^2\eta^2)U_n = 0 \quad , \tag{18a}$$

and the same equation for $V_n(\xi)$. The boundary condition $E_\eta = 0$ is now

$$\left.\frac{\partial V_n}{\partial \xi}\right|_{\xi=\xi_o} = 0 \quad . \tag{18b}$$

The eigenvalue $\lambda_n = \lambda_{1n}$ is the one from the usual spheroidal equation, and they are known, (eg. Reference 3, Page 29, reproduced in Table 1). The resonance frequencies are probably given in Reference 4, but this reference is not easily assessible.

The simpler estimates performed in the initial stages of the field and energy transfer calculations, (eg. Reference 5) compare favorably to the exact electromagnetic fields given above, and to the energy transfer calculations that follow. First, let us determine the frequency from the boundary condition, $E_\eta = 0$; with equation (14),

$$\frac{\partial}{\partial \xi}\left[\sqrt{\xi^2-1}\ R_{1n}(h,\xi)\right] = 0 \quad : \tag{19}$$

in a future numerical calculation we will solve for the frequency parameter $h = h_n(\xi_o)$ as function of axial mode number n and cavity wall location ξ_o. Here the WKB approximation given in Reference 1, Section 3.91, will be used. Approximately,

$$\sqrt{\xi^2-1}\ R_{1n}(h,\xi) \simeq \left(\frac{\pi}{2h}\right)^{\frac{1}{2}} \left(\frac{s}{s'}\right)^{\frac{1}{2}} J_1(s) \quad , \tag{20a}$$

where J_1 is the Bessel function of first order,

$$s = s(h,n;\xi) \simeq h\sqrt{\xi^2-1} - \frac{q}{2}\arccos \xi^{-1} - \frac{q^2+3}{16h\xi^2}\sqrt{\xi^2-1} \quad , \tag{20b}$$

and $q = 2n-1$. The factor $(s/s')^{\frac{1}{2}}$ is a slowly varying function of ξ, viz.

$$\frac{s}{s'} = \frac{\xi^2-1}{\xi}\ \frac{1 - \frac{q^2+3}{16h^2\xi^2} - \frac{q}{2h}\frac{\arccos \xi^{-1}}{\sqrt{\xi^2-1}}}{1 - \frac{q}{2h\xi^2} + \frac{(q^2+3)(\xi^2-2)}{16h^2\xi^3}} \quad ; \tag{21}$$

for $\xi>>1$ this becomes approximately $s/s' = \xi$. Therefore it is reasonable to ignore this factor in (20a). The boundary condition $E_\eta = 0$ then yields the result

$$s = j'_{1,\ell} \quad ; \tag{22}$$

or approximately, neglecting the last term

$$h_1 = h = (\xi_o^2-1)^{-\frac{1}{2}}\ \left(j'_{1\ell} + \frac{2n-1}{2}\arccos \xi_o^{-1}\right) \quad ; \tag{23a}$$

Not neglecting the last term gives $h_2 = \frac{1}{2}\left(h_1 + \sqrt{h_1^2 + (q^2+3)/4\xi_o^2}\right)$.

Here $\ell = 1$ corresponds to a half-wave cavity, and $\ell = 2$ to a 3/2-wave cavity.

The exact electric field along the axis is

$$E_\eta = E_p N_n (1-\eta^2)^{-\frac{1}{2}} S_{1n}(h,\eta) \quad , \tag{24}$$

where E_p is the peak field value, and N_n is a normalization constant. Asymptotically, for $h>>1$, in a region of width $h^{-\frac{1}{2}}$ about zero[7]

$$E_\eta = E_p N_n H_r (\eta\sqrt{h}) \exp - h\,\eta^2/2 \quad , \tag{25}$$

where $r = n-1$ (in general, $S_{mn} \sim H_{n-m}$) .

The previous estimates of the energy transfer were based on equation (25), but with $r = n$; however, in that case the frequency estimate, h_e, was given by

$$h_e = (\xi_o^2-1)^{\frac{1}{2}} \left[j_{o\ell} + \frac{2n+1}{2} \arccos \xi_o^{-1} \right] \quad . \tag{26a}$$

Hence for a corresponding field pattern, n in equation (26) should be replaced by $n-1$; then the difference between equations (23) and (26a) is

$$\Delta h_\ell = j_{o\ell} - j'_{1\ell} \quad : \tag{26b}$$

the first two values are $\Delta h_1 = 0.56$ and $\Delta h_2 = 0.19$, for a relative change in frequency $\Delta h/h$ less than about 10%. The conclusion here is that the energy transfer as computed previously is consistent with a parallel compulation using the more accurate vector electric fields.

A conclusive energy transfer calculation must be done with accurate numerical data on the spheroidal functions, and their zeroes. These calculations are underway, but for the moment it is reasonable to trust the previous energy transfer rates. It should be mentioned, however, that the approximation to the axial spheroidal function $S_{n1} \sim H_{n-1}$ exp . . . is not strictly valid[7] in the region of exponential decrease $|n\sqrt{h}|>>1$, and this fact could effect the energy transfer calculation.

$E_\perp$ at the cavity wall.

An important quantity is the normal field at the cavity wall. Elsewhere it is shown that the parallel electric field, or rather the equivalent magnetic field at the wall, can be up to 10^9 V/m, while electrical breakdown sets in at 30 times lower values, approximately 3×10^7 V/m. Therefore it is important that $E_\perp/E_{//}$ be small.

The ratio between the normal field at the wall and the parallel field along the axis is given by equation (16). This formula is being evaluated, and the results will be given in another appendix: here an estimate of $E_\perp/E_{//}$ will be given with simple physical considerations. Namely the existence of a spatial magnetic field pattern on the cavity wall leads to a comparable surface current pattern, hence to a surface charge density which finally generates the normal field.

Figure 3 gives the accelerating cavity with the directions of the main field components $E_{//}$ along the axis, and B_ϕ in the midplane parallel to the cavity wall. The surface current J induced in the wall is approximately given by

$$B_\phi \simeq \mu_o J \quad , \tag{27}$$

found by integrating the magnetic field along the sides of the rectangle given in Figure 4a. The spatial dependence of the $B_\phi = B_\phi(\eta)$ gives the charge accumulation Q in the cube of Figure 4b:

$$J \simeq \ell_{//} \frac{d\sigma}{dt} \simeq \ell_{//}\, \omega\, \sigma \quad ; \tag{28}$$

here $\ell_{//}$ is a typical length scale in the variation of B_ϕ, σ is the surface charge, and ω^{-1} is a typical time scale. The surface charge gives the normal electric field according to

$$E_\perp = \frac{\sigma}{\epsilon_o} \quad . \tag{29}$$

The normal electric field at the cavity wall $E_\perp$, compared to the peak parallel electric field $\lambda/4$ away from the wall, $E_\parallel = c\, B_\phi$,

$$E_\perp/E_\parallel \simeq (\ell_\parallel k)^{-1}$$

where $k = \omega/c$ is the free-space wavenumber.

The above estimate shows that the large fields predicted for the transverse RF accelerator are obtainable when the free-space wavelength is small compared to the wavelength of the fields on the wall.

The accelerating field along the axis in the cavity center is the parallel field at the wall times an additional radial factor $4R/\lambda$, where R is the cavity radius and λ is the wavelength. The magnetic field B_ϕ goes with radius r roughly as $1/r$ because $\int \underline{B}.d\underline{\ell} = 2\pi\, r\, B_\phi(r)$ is a constant, for each integration path along the maximum of B_ϕ. The electric field in the center is roughly equal to cB_ϕ along the smallest integration path encircling the center, at $r = \lambda/4$. Therefore the normal field at the wall $E_\perp$ is, compared to the accelerating field $E_\parallel$ on axis,

$$E_\perp/E_\parallel \simeq \lambda^2/8\pi\ell_\parallel R \quad . \tag{31}$$

Therefore the breakdown limitation can be avoided by using wavelengths short compared to the cavity dimensions. An estimate based on the exact formula (16), gives elesewhere, is in general agreement with (31).

CAVITY LOADING

The electron beam that is accelerated by a particular externally excited cavity mode can itself excite other cavity modes. These modes, once built up to large amplitudes, have their own, probably deleterious, influence on the accelerating beam. The mode excitation due to a prescribed electron beam is given in the sequel.

Various important simplications are made. The beam electrons are relativistic, and therefore they keep their velocity approximately constant, equal to the light speed c. This approximation necessarily ignores any radiation from beam acceleration; most of the radiation is peaked in the forward direction, and will escape from the cavity. It will be treated in a separate calculation.

The beam is supposed to be injected into the cavity along the z-axis, preserving the azimuthal symmetry already imposed on the accelerating mode. Then the magnetic field generated by the beam current will be in the same direction as the cavity mode field, namely the azimuthal direction.

The above considerations allow simplification of the full inhomogeneous vector wave equation to an inhomogeneous scalar wave equation for the magnetic field $\underline{B} = \underline{e}_\phi\, b$ (See equation 17 sqq.)

$$\nabla^2 b - \frac{1}{r^2} b - \frac{\partial^2 b}{\partial t^2} = C, \qquad (32)$$

where $\underline{e}_\phi$ is the unit vector in the azimuthal direction, and C is the $\underline{e}_\phi$ - component of the curl of the current source term,

$$\underline{e}_\phi \; C(\underline{x},t) = \mu_o \, c \, \nabla \times \underline{e}_z \; j(\underline{x},t) \tag{33}$$

where $j(\underline{x},t)$ is the current density. A reasonable functional form for the n'th electron bunch is

$$j_n(x,t) = \frac{I_p}{2L_r^2} \exp\left[- (z_n - ct)^2/2L_z^2 - (x^2+y^2)/2L_r^2 \right] \tag{34}$$

where I_p is the peak current, L_r is a typical width in the radial direction, z_n is the center of the particle bunch along the cavity axis, with a typical bunch length L_z. It is easy to verify that $\nabla \times \underline{j}$'s only component indeed points in the $\underline{e}_\phi$ - direction.

A suitable set ψ_n of real eigenfunctions for the cavity is found above. The inhomogeneous equation (32) is then solved by

$$b(\underline{x},t) = \int G(\underline{x},t;\underline{x}_o,t_o) \quad C(\underline{x}_o,t_o) \quad , \tag{34}$$

where the Green's function G can be expanded in terms of the eigenfunctions (e.g. Reference 6, equation 7.3.24)

$$b = c^2 \sum_j \psi_j(x)/\omega_j \int_o^t dt_o \, \sin\left[\omega_j(t-t_o)\right] \int dV_o \psi_j(\underline{x}_o) \; C(\underline{x}_o,t_o) \; , \tag{35}$$

Here the summation is over all indices of the eigenfunctions, for the cavity $j = (n,\ell)$.

These expressions basically say that each mode ψ_n is excited by the source C with a coupling strength that depends on the spatial overlap of the mode with the source, and on the temporal overlap. All that is left to do is to evaluate these overlap integrals explicitly. When this is done one can go back and consider the effect of these beam-excited modes on the beam itself.

In the evaluation are needed the explicit forms of the eigenfunctions, the current, and the frequencies. The eigenfunctions are given in equation (11):

$$\psi_j(\underline{x}) = \Lambda_{n\ell} \; S_{1n}(h,\eta) \; \bar{R}_{1n}(h_{n\ell},\xi) \quad , \tag{36}$$

where $\Lambda_{n\ell}$ is the normalization constant.

h is the eigenvalue, related to the frequency by $h = \frac{f\omega}{2c}$; its indices $(h \equiv h_{1n\ell})$ are omitted. The eigenvalue satisfies

$$0 = \frac{\partial}{\partial\xi}\left[(\xi^2-1)^{\frac{1}{2}} R_{1n}(h_{n\ell},\xi)\right] \quad . \tag{37}$$

The source $C(x_o,t_o)$ in spheroidal coordinates is

$$C(\xi,\eta,t) = -\frac{\mu_o c I_p}{f L_r^2} \sqrt{\frac{(\xi^2-1)}{\xi^2-\eta_j^2}} \frac{\partial}{\partial\xi}\left[\sqrt{\xi^2-\eta^2}\, \exp-\left(\frac{f}{2}\xi\eta - ct\right)^2/2L_z^2 \right.$$
$$\left. \exp-\left(\frac{f}{2}\right)^2 (\xi^2-1)\,(1-\eta^2)/2L_r^2\right] \quad . \tag{38}$$

Notice that this formula is for one electron bunch only: for N bunches there is another summation over bunches, indexed by j, say: $C = \Sigma_j C_j$.

With these expressions it is, in principle, possible to evaluate equation (35); however, the calculations are terribly messy and they are not performed now. Instead, we make the following physical arguments in an attempt to search an acceptable conclusion.

The first observation is that the spatial overlap integral can be approximated in two limits, one in which a typical length scale of the eigenfunctions is much larger than the scale of the charge bunch; the other limit applies when the opposite is true. These are the low and high mode number cases, respectively. In the first case the integral is approximately constant, in the second case the integral is zero. The upshot here is that only a finite number of modes is coupled to the source and that the coupling constants are all of the same order. In this connection, notice that the normalization constant is of order (peak value of the function x integration interval)$^2/_2$, hence that the normalization and peak value cancel each other, except perhaps for some dependence on the integration interval in the normalization.

It is a different story for the time integration. Here the coupling involves, mainly,

$$\psi \sim \sum_j \int_0^t dt_o \sin\left[\omega_{n\ell}\,(t-t_o)\right] \exp - \left(\frac{f}{2}\,\eta_j - ct\right)^2/_2 L_z^2 \quad , \qquad (39)$$

which can be large only when the correct bunch spacings $\eta_{j-1}-\eta_j$ relative to the frequency of the accelerating mode are obtained. Otherwise, the integrand in (39) will be oscillatory, and vanish when integrated over many bunches: one bunch may excite a mode to a certain, small, amplitude, but the next bunch, or a bunch a few further down the line, will take the energy from this mode: the net result is little excitation of extraneous modes.

The above scenario is reasonable if the frequencies are incommensurate. This is highly likely, but untested at the moment. The best estimate gives for the frequency a linear expression in terms of Bessel functions zeroes: these are certainly incommensurate.

Our conclusion is that modes other than the accelerating mode can be excited in the cavity, but that these modes remain at a relatively low level. Therefore they will have a minor effect on particle acceleration in the transverse RF accelerator.

Further Analytical Estimates.

The total electromagnetic energy W in the cavity can be easily estimated as

$$W = \frac{\epsilon_o}{2} E_p^2 V$$

times a geometrical factor; E_p is the peak field, V is the volume. The geometrical factor of order unity must be evaluated using the particulars of each cavity. Remember that in radiation field the time-averaged electric and magnetic field energies are equal,

$$\epsilon_o \int |\underline{E}|^2 \, dV = \mu_o^{-1} \int |\underline{B}|^2 \, dV \quad , \tag{40}$$

and therefore it is sufficient to evaluate the least cumbersome of these expressions.

The maximum magnetic field energy, equal to the total E-M energy W, becomes in spheroidal coorinates:

$$W = \left(\frac{f}{2}\right)^3 \frac{2\pi}{2\mu_o} B_p^2 N_p^2 \int_1^{\xi_o} d\xi \int_{-1}^{1} d\eta \, (\xi^2-\eta^2) \, S_{ln}^2 (h,\eta) \, R_{ln}^2 (h_{n\ell}, \xi) \tag{41}$$

Here B_p is the peak magnetic field, and the double integral with henceforth be denoted by I. N_p is a normalization constant to be discussed later Equation (41) clearly displays the expected form, an energy density $B_p^2/2\mu_0$ times a volume (for a confocal cavity, the diameter is equal to the focal distance f, hence in this case $V = \pi f^3$), times a geometrical factor given by the remaining factors.

The double integral can be split in two terms with $\xi^2-\eta^2 = (\xi^2-1) + (1-\eta^2)$:

$$I = \int_1^{\xi_0} d\xi\ (\xi^2-1)\ R_{1n}^2\ (\ h_{n\ell_j}\xi\ )\int_{-1}^{1} d\eta\ (1-\eta^2)\ S_{1n}^2\ (h,\eta)$$

$$+\ \int_1^{\xi_0} d\xi\ R_{1n}^2\ (\ h_{n\ell_j}\xi\ )\int_{-1}^{1} d\eta\ (1-\eta^2)\ S_{1n}^2\ (h,\eta)\quad . \qquad (42)$$

It is convenient to choose the normalization

$$\int_{-1}^{1} d\eta\ S_{1n}^2\ (h,\eta) \ = \ 1 \qquad ; \qquad (43)$$

Note that this normalization differs from the one used by others, eg.

$\int d\eta \ldots = \frac{(n+1)}{(n+\frac{1}{2})(n-1)n}$ as used by Meixner and Schafke:

these notational difficulties are a recurring nuisance. The remaining η - integral is

$$\int_{-1}^{1} d\eta\ (1-\eta^2)\ S_{mn}^2(h,\eta) = \frac{\partial \Lambda_n}{\partial h^2} \qquad , \qquad (44)$$

where Λ_n is the eigenvalue in the spheroidal differential equation

$$\left[\frac{d}{d\eta}\ (1-\eta^2)\ \frac{d}{d\eta} + q\ (\Lambda,h^2,\eta;m)\right] S_{mn}\ (h,\eta) = 0 \qquad , \qquad (45a)$$

where

$$q = -\ \Lambda_n + h^2\ (1-\eta^2) - \frac{m^2}{1-\eta^2} \qquad . \qquad (45b)$$

Series for Λ_n in powers of h^2 are well-known and this fact makes relation (44) useful. Its proof is simple: multiply equation (45a) for h_0 with $S_{mn}\ (h_1,\eta)$ belonging to $h_1^2 = h^2+\Delta h^2$, interchange the subscript 0 and 1, subtract and integrate over the interval $\left[-1,1\right]$. The result is

$$0 = (\Delta h^2)^{-1} \int d\eta \left[q(\Lambda_0, h_0^2, \eta; m) - q(\Lambda_1, h_1^2, \eta; m) \right] S_{mn}(h_0, \eta)\ S_{mn}(h_1, \eta) \quad ; \quad (46)$$

Taking the limit $\Delta h^2 \to o$ gives

$$\int d\eta\ \frac{\partial q}{\partial h^2}\ S_{mn}^2\ (h, \eta) = 0 \quad , \quad (47a)$$

which is equation 44 when using the explicit form for q, equation 45b.

The eigenvalue λ_{mn} in Table 1 is related to Λ by $\Lambda = h^2 - \lambda_{mn}$; hence equation (44) becomes

$$\int_{-1}^{1} d\eta\ (1-\eta^2)\ S_{mn}^2\ (h, \eta) = 1 - \frac{\partial \lambda_{mn}}{\partial h^2} \quad . \quad (48)$$

In the limit $h^2 \to \infty$, when $S_{mn}^2\ (h, \eta)$ goes to a δ -function (or derivatives thereof), equation (48) becomes unity, in agreement with Table 1.

The integrals over the radial coordinates ξ_o satisfy a relation of the same form, but with an extra term:

$$\int_{1}^{\xi_0} d\xi\ (\xi^2-1)\ R_{mn}^2\ (h, \xi) = \frac{\partial \lambda_{mn}}{\partial h^2} - 1 + \frac{\partial^2 \left[\sqrt{\xi^2-1}\ R_{mn} \right]}{\partial \xi \partial h^2} \Bigg|_{\xi=\xi_o} \quad . \quad (49a)$$

This last term is related to the non-zero boundary condition on R_{mn}. This term can be written another way. A change in the parameter h (frequency) implies a different coordinate $\xi_o = \xi_o\ (h^2)$ where E_η vanishes (see equation 19).

Then $\partial / \partial h^2$ can be replaced by $\partial \xi_o / \partial h^2 \times \partial / \partial \xi$, and the second derivative becomes, $\partial^2 / \partial \xi^2$: This in turn, can be re-written with equation (10). The result is

$$I_{mn\ell} = \frac{\partial^2 \sqrt{\xi^2-1}\, R_{mn}}{\partial\xi \partial h^2}\bigg|_{\xi=\xi_o} = \frac{\partial \xi_o(h^2)}{\partial h^2} \frac{\lambda_{mn}-h^2\xi_o^2}{\sqrt{\xi_o^2-1}} R_{mn}(h, r_{n\ell}) \quad . \tag{49b}$$

The integral I (equation 42) becomes simply

$$I = I_{1n\ell} \quad , \tag{50a}$$

and the total E-M energy in the cavity is

$$W = \left(\frac{f}{2}\right)^3 \frac{\pi}{\mu_o} B_p^2 N_p^2 I_{1n\ell}^2 \quad . \tag{50b}$$

The final ingredient in this formula is the normalization constant N_p (and the numerical evaluation of equation 49b).

The normalization constant N_p for the magnetic field is defined by

$$B_\phi = B_p N_p R_{1n} S_{1n} \quad , \tag{51}$$

where B_p is the peak value of the magnetic field, and S_{1n} and R_{1n} are normalized to unity according to equation (43), and the corresponding equation for R. Given this normalization one needs to find the maximum of $S_{1n}(h,\eta)$ over $|\eta| \leq 1$ and of $R_{1n}(h,\xi)$ over $1 \leq \xi < \xi_o$

In the axial direction a local maximum occurs at all zeroes z'_ℓ of $S_{1n}/d\eta$; however, the absolute maximum takes place for the largest of these, $z'_m = \max_\ell (z'_\ell)$. This can be easily argued from WKB-theory. Hence,

$$S_{1n}(h,\eta)\Big|_{max} = S_{1n}(h, z'_m) \quad , \tag{52a}$$

where z'_m is the largest zero of

$$\frac{\partial S_{1n}(h,z'_m)}{\partial \eta} = 0 \quad . \tag{52b}$$

In the radial direction the maximum occurs closest to the center $\xi=1$. This is evident from the basic $1/r$ dependence of cylindrical coordinates, and can also be argued on WKB grounds. Hence,

$$R_{1n}(h,\eta)\Big|_{max} = R_{1n}(h, r'_{n1}) \quad , \tag{53a}$$

where r'_{n1} is the first zero of

$$\frac{dR_{1n}(h,r'_{n1})}{d\eta} = 0 \quad . \tag{53b}$$

The normalization constant N_p is then

$$N_m = \left[R_{1n}(h,r'_{n1})\, S_{1n}(h,z'_m)\right]^{-1} \quad . \tag{54}$$

The hooker in all this is that the spheroidal functions are not well tabulated, their zeroes are not well-known, etc. These numerical data need to be calculated before one can determine the numerical value of the various quantities such as equations (54) and (16).

REFERENCES

1. J. Meixner and F. M. Schafke, "Mathematischen Funktionen and Spharoidfunktionen", Springer, 1954.

2. W. K. H. Panofski and M. Phillips, "Classical electricity and Magnetism", 2nd Edition; Addition-Wesley, 1962.

3. C. Flammer, "Spheroidal Wave Functions", Standford, 1957.

4. T. Nimura, "Resonance Frequency of Spheroidal Cavity Resonator", Sci. Rep. Res. Inst. Tôhoku Univ. 1/2, 73-90, (1951).

5. Western Research Internal Report V-156, October 1980.

6. P. M. Morse and H. Feshbach, "Methods of Theoretical Physics", McGraw Hill, 1953.

7. D. Slepian, "Some Asymptotic Expansions For Prolate Spheroidal Wave Functions", J. Math and Phys. 44 99 (1965).

TABLE 1

The eigenvalues λ_{1n} for the spheroidal wave equation as function of the parameters $c = h = fk/2$.

λ_{1n}

$$\lambda_{11} = 2 + \frac{1}{5}c^2 - \frac{4}{875}c^4 + \frac{8}{65,625}c^6 - \frac{124}{58,953,125}c^8 - \ldots$$

$$\lambda_{12} = 6 + \frac{3}{7}c^2 - \frac{4}{1,029}c^4 + \frac{8}{554,631}c^6 + \frac{5,420}{9,539,098,569}c^8 - \ldots$$

$$\lambda_{13} = 12 + \frac{7}{15}c^2 + \frac{152}{111,375}c^4 - \frac{115,568}{977,315,625}c^6 + \frac{34,094,936}{15,964,450,734,375}c^8 + \ldots$$

$$\lambda_{14} = 20 + \frac{37}{77}c^2 + \frac{7,064}{5,934,929}c^4 - \frac{462,736}{35,188,194,041}c^6 - \frac{339,769,051,816}{599,396,295,493,692,697}c^8 + \ldots$$

$$\lambda_{15} = 30 + \frac{19}{39}c^2 + \frac{1,108}{1,245,699}c^4 - \frac{301,160}{96,630,117,129}c^6 - \frac{69,222,847,348}{2,052,497,609,859,563,685}c^8 - \ldots$$

$$\lambda_{16} = 42 + \frac{27}{55}c^2 + \frac{5,684}{8,485,125}c^4 - \frac{495,016}{487,682,559,375}c^6 - \frac{5,894,701,468}{2,302,259,141,535,890,625}c^8 - \ldots$$

$$\lambda_{17} = 56 + \frac{109}{221}c^2 + \frac{1,167,376}{2,255,916,949}c^4 - \frac{132,492,064}{330,543,719,118,327}c^6 + \frac{3,149,302,579,970,160}{5,406,455,219,158,600,211,866,547}c^8 - \ldots$$

$$\lambda_{18} = 72 + \frac{47}{95}c^2 + \frac{31,984}{78,021,125}c^4 - \frac{96,594,016}{534,442,755,721,875}c^6 + \frac{16,316,385,212,272}{23,965,276,291,519,365,828,125}c^8 - \ldots$$

For general m and n : $q = 2n - 2m + 1$, $\gamma = h$

(Meixner & Schafke, Section 3.25):

$$2h^2 - \lambda_{mn}(h) = \gamma q + m^2 - \frac{1}{8}[q^2 + 5] - \frac{q}{64\gamma}[q^2 + 11 - 32m^2] -$$
$$- \frac{1}{1024\gamma^2}[5(q^4 + 26q^2 + 21) - 384m^2(q^2 + 1)] -$$
$$- \frac{1}{\gamma^3}\left[\frac{1}{128 \cdot 128}(33q^5 + 1594q^3 + 5621q) - \frac{m^2}{128}(37q^3 + 167q) + \frac{3m^4}{8}q\right] -$$
$$- \frac{1}{\gamma^4}\left[\frac{1}{256 \cdot 256}(63q^6 + 4940q^4 + 43327q^2 + 22470) -\right.$$
$$\left. - \frac{m^2}{512}(115q^4 + 1310q^2 + 735) + \frac{3m^4}{8}(q^2 + 1)\right] -$$
$$- \frac{1}{\gamma^5}\left[\frac{1}{1024 \cdot 1024}(527q^7 + 61529q^5 + 1043961q^3 + 2241599q) -\right.$$
$$- \frac{m^2}{32 \cdot 1024}(5739q^5 + 127550q^3 + 298951q) +$$
$$\left. + \frac{m^4}{512}(355q^3 + 1505q) - \frac{m^6}{16}q\right] + O(\gamma^{-6})$$

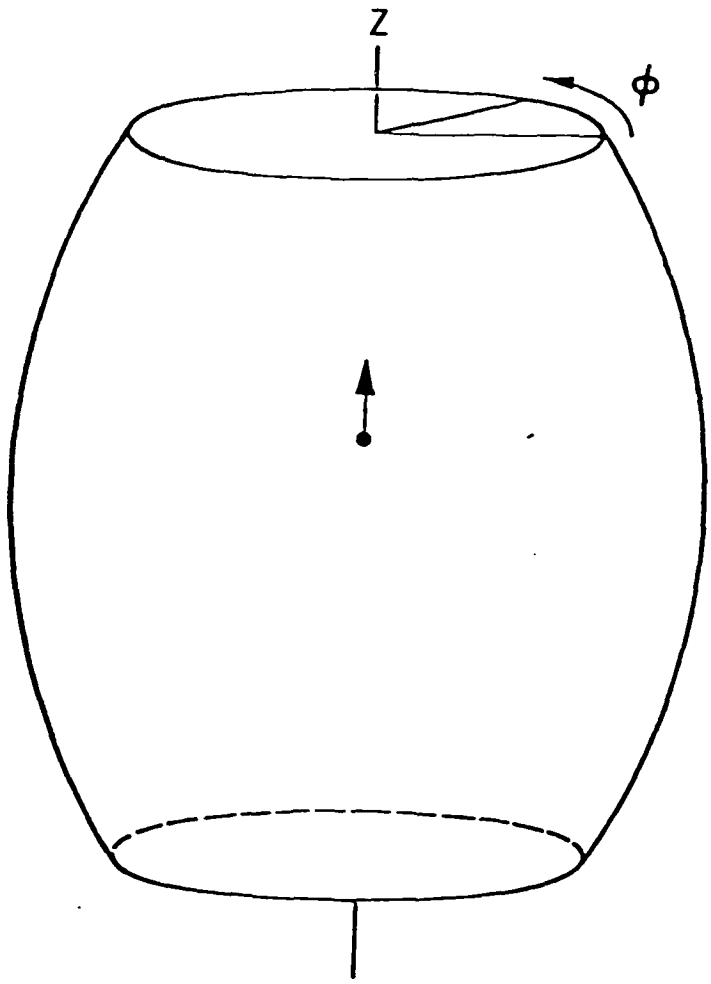

Figure 1. Transverse RF accelerator cavity.

$1 < \xi < \infty,$

$-1 < \eta < 1,$

$0 \leq \phi < 2\pi$

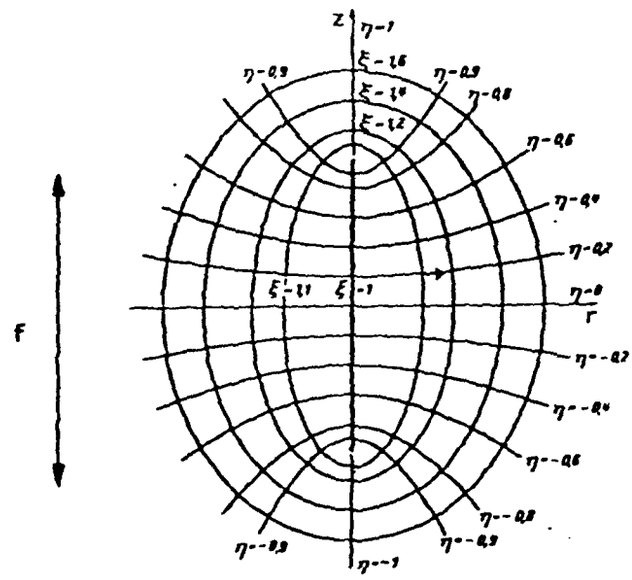

Figure 2. Prolate Spheroidal Coordinates.

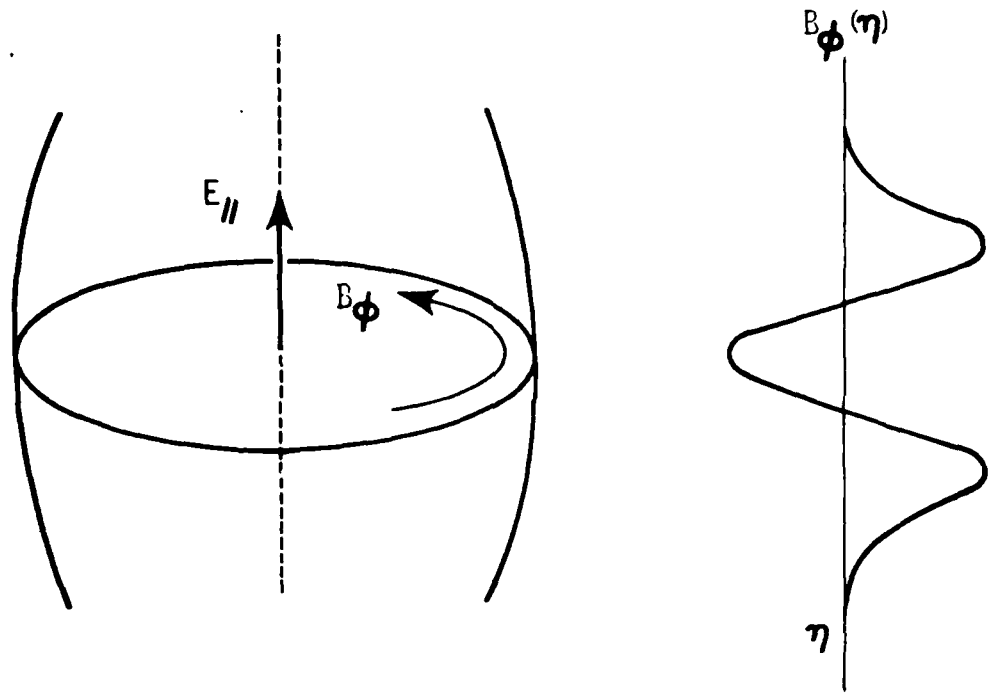

Figure 3.

The transverse RF accelerator cavity with the major electromagnetic field components.

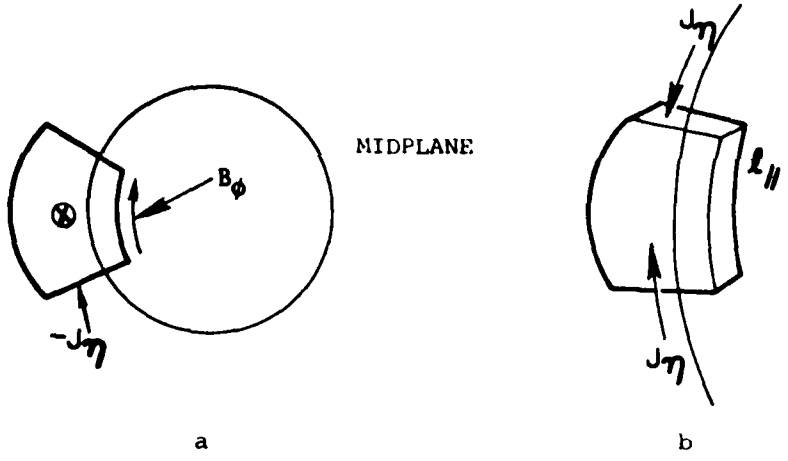

Figure 4.

The surface and volume elements used to determine the normal electric field.

APPENDIX III

Normal Fields With Exact Mode Structure

The transverse RF accelerator allows, in principle, extremely high accelerating gradients because the accelerating electric fields are mainly parallel to the cavity wall. The parallel field is then limited by Joule heating to about 10^9 V/m . This value is much higher than the maximum normal field that can be sustained, $E_\perp \leq 3 \times 10^7$ V/m . This section evaluates the exact expression for the normal field at the wall, compared to the accelerating field along the cavity axis.

The expression to be calculated is

$$\frac{E_\xi\,|_{\text{wall, max}}}{E_\eta\,|_{\text{axis, max}}} = \frac{R_{1n}(h,\xi_o)}{\frac{\partial}{\partial\xi}\left[\sqrt{\xi^2-1}\;R_{1n}(h,\xi)\right]_{\xi=1}} \times \frac{\left\{\frac{1}{\sqrt{\xi^2-\eta^2}}\frac{\partial}{\partial\eta}\left[\sqrt{1-\eta^2}\;S_{1n}(h,\eta)\right]\right\}_{\max}}{\left\{\sqrt{1-\eta^2}\;S_{1n}(h,\eta)\right\}_{\max}} \qquad (1)$$

(Equation 16 of "Electromagnetic fields in Ellipsoidal Cavity"). It consists of a radial part, with independent variable ξ , and an axial part, with variable η . Let us consider these factors separately, using the asymptotic form of R and S for large frequency $\left(h = \frac{f\omega}{2c} \gg 1\right)$.

The radial eigenmode R_{1n} is approximately

$$R_{1n}(h,\xi) = \left(\frac{\pi}{2h}\right)^{1/2} \sqrt{\frac{1}{\xi^2-1}} \left(\frac{s}{s'}\right)^{1/2} J_1(s) \quad , \tag{2a}$$

where to lowest order in h

$$s = h\sqrt{\xi^2-1} \quad , \tag{2b}$$

and J_1 is the Bessel function of first order.

The frequency is related to the coordinate ξ_o of the wall by the implicit relation

$$\frac{\partial}{\partial\xi}\left[\sqrt{\xi^2-1}\ R_{1n}(h,\xi)\right]_{\xi=\xi_o} = 0 \quad . \tag{3}$$

Using the approximation (2a) this condition takes place approximately when J_1' vanishes, or equivalently, at the maximum of J_1. In the region $s>>$ this maximum is simply the dominant term in the asymptotic expression of J_1:

$$J_{1\ max} \simeq \sqrt{\frac{2}{\pi h}}\ (\xi_o^2-1)^{-1/4} \quad . \tag{4}$$

The additional factor is

$$\frac{s}{s'} \simeq \frac{\xi_o^2-1}{\xi_o} \quad . \tag{5}$$

The value of the ξ-dependent denominator in Equation (1) can be found in the opposite limit $J_1(s) \simeq s/2$ for $s \longrightarrow 0$. Then

$$\frac{\partial}{\partial \xi} \sqrt{\xi^2-1}\ R_{1n}(h,\xi)\Big|_{\xi=1} = \left(\frac{\pi}{2h}\right)^{1/2} h \quad ; \tag{6}$$

hence

$$\frac{R_{1n}(h,\xi_o)}{\frac{\partial}{\partial \xi}\sqrt{\xi^2-1}\ R_{1n}(h,\xi)\Big|_{\xi=1}} = \sqrt{\frac{2}{\pi}}\, h^{-3/2}\, \xi_o^{-1/2}\, (\xi_o^2-1)^{-1/4} . \tag{7}$$

The axial factor can be evaluated from the WKB expression for the function

$$\sqrt{1-\eta^2}\ S_{1n}(h,\eta) \simeq H_{n-1}(\eta\sqrt{h})\ \exp - h\eta^2/2 \quad ; \tag{8a}$$

in this expression one can ignore the factor $\sqrt{1-\eta^2}$, at least for those large values of h for which (8) is valid. The differential equation for (8) is

$$g_n'' + Q(n,x) g_n = 0 \quad , \tag{8b}$$

where $x = \eta\sqrt{h}$, and $Q(n,x) = 2n-1-x^2$.

The extremes of the function S_{1n} lie between the turning points; in fact, the maximum is the local maximum closest to the turning point. In contrast, the maximum of the derivative occurs in the middle between the turning points. This can be shown easily from the WKB-expansion about the turning point, $x = x_t + \Delta x$:

$$g_n \simeq \sqrt{\pi}\ a^{-1/6}\ \mathrm{Ai}(a^{1/3}\Delta x) \quad , \tag{9a}$$

where $a = -\partial Q/\partial x$ at the turning point, and Ai is the Airy function. The maximum occurs at the maximum of $Ai(t) = 0.5356$, at $t = 1.003$.

The derivative is calculated with the WKB-expression between turning points:

$$g_n(x) = Q^{-\frac{1}{4}} \cos\left[\int\sqrt{Q}\,dx\right] \quad , \quad \ldots \tag{9b}$$

with derivative

$$g' = Q^{\frac{1}{4}} \sin\left[\int\sqrt{Q}\,dx\right] \quad . \tag{9c}$$

The maximum of this is obviously where Q is largest, at $x = 0$.

The maximum (9a) becomes, using the turning point $x = \sqrt{2n-1}$,

$$g_{n,max} = \frac{\sqrt{\pi}\,Ai(max)}{2^{\frac{1}{4}}(n-\frac{1}{2})^{1/12}} \quad , \tag{10a}$$

while the maximum of the derivative becomes

$$g'_{n,\,max} = (2n-1)^{\frac{1}{4}} \quad , \tag{10b}$$

The axial factor becomes finally, using $\partial/\partial\eta = \sqrt{h}\,\partial/\partial x$ and setting $\eta = 0$ in the square roots that multiply S_{1n}:

$$\frac{\left\{(\xi_o^2-\eta^2)^{-\frac{1}{2}}\frac{\partial}{\partial\eta}\left[\sqrt{1-\eta^2}\,S_{1n}(h,\eta)\right]\right\}_{max}}{\left\{(1-\eta^2)^{-\frac{1}{2}}\,S_{1n}(h,\eta)\right\}_{max}} = \sqrt{h}\,\frac{(n-\frac{1}{2})^{\frac{1}{3}}}{\sqrt{8\pi}\,Ai(max)\,\sqrt{\xi_o^2-1}} \quad . \tag{10c}$$

The ratio between normal field at the wall, and accelerating field

along the axis, Equation (1), becomes from (7) and (10):

$$\frac{E_\perp}{E_\parallel} \simeq \left[\frac{\pi}{2}\mathrm{Ai(max)}\right]^{-1} \frac{(n-\frac{1}{2})^{1/3}}{h\xi_o^{\frac{1}{2}}(\xi_o^2-1)^{\frac{3}{4}}} \quad : \tag{11}$$

The coefficient $\left(\frac{\pi}{2}\mathrm{Ai\ (max)}\right)^{-1} \simeq 0.3$.

The conclusion from this formula is that the normal fields remain small compared to the accelerating fields by a combination of high frequencies $h = \frac{f\omega}{2c}$, high axial mode number n , and large wall distance ξ_o . However, none of these factors is clearly dominant, although increasing the frequency is most effective.

The formula (11) agrees approximately to the previous estimate, Equation (31) in Appendix I:

$$\frac{E_\perp}{E_\parallel} \simeq \frac{\pi}{2} \frac{c^2}{\omega^2} \frac{1}{\ell_\parallel R} \quad . \tag{12}$$

When Equations (11) and (12) are written in corresponding quantities the discrepancies become clear. For example, Equation (12) becomes, using $h = \frac{f\omega}{2c}$, $R = \frac{f}{2}\sqrt{\xi_o^2-1}$, and $\ell_\parallel$ the typical wavelength on the axis $(\lambda n^{-\frac{1}{2}})$ times a factor from the projection on the cavity wall, $\ell_\parallel \simeq \lambda\xi\eta^{-\frac{1}{2}}$

$$\frac{E_\perp}{E_\parallel} \simeq \frac{n^{\frac{1}{2}}}{4h\ \xi_o\sqrt{\xi_o^2-1}} \tag{13}$$

These formulas are in good agreement; the frequency dependence is h^{-1} in both, and at least for ξ_o large the formulas go as ξ_o^{-2} ,

but the axial mode number dependence is $n^{1/3}$ versus $n^{\frac{1}{2}}$. It should be noted, however, that both Equations (11) and (13) contain various approximations that might explain part of the discrepancy.

Numerically, it appears that, for $\xi_o = \sqrt{2}$,

$$\frac{E_\perp}{E_\parallel} \simeq 0.5 \frac{(n-\frac{1}{2})^{2/3}}{h} , \qquad (14)$$

only a factor $n^{1/6}$ off from (13) but different by $n^{1/3}$ from (11). The reason is probably that the influence of the axial mode number on the frequency is entirely neglected in Equation (2b).

The cavity parameters that determine the normal fields at the wall are the wavelength λ compared to the focal distance of the cavity f, $h^{-1} = \lambda/(\pi f)$, and the cavity shape as parameterized by ξ_o. The axial mode number n has a minor influence.

APPENDIX IV

Acceleration and Emittance Calculations

The exact electromagnetic cavity modes discussed earlier determine the acceleration of relativistic particles shot into the cavity. Three terms in the Lorentz force that need to be evaluated are:

$$\frac{dp_{\parallel}}{dt} = e\, E_{\parallel}\left[z(t)\right] \exp - i\omega t \quad , \tag{1a}$$

$$\frac{dp}{dt}_{\perp}, E = e\, E_{\perp}\left[z(t)\right] \exp - i\omega t \quad , \tag{1b}$$

$$\frac{dp}{dt}_{\perp}, B = - eB_{\phi}\left[z(t)\right] \exp - i\omega t \quad , \tag{1c}$$

the last term coming from $\underline{v}_{\eta} \times \underline{B}_{\phi}/c = - \underline{e}_{\xi} B_{\phi}$. The field should be taken at the actual position of the particle, $z = z(t)$. The magnetic and electric fields are given as a product of two spheroidal wave functions and their derivatives:

$$B_{\phi}(\xi,\eta) = \text{const.}\ R_{1n}\ (h,\xi)\ S_{1n}\ (h,\eta) \quad , \tag{2a}$$

where h is the parameter

$$h = \frac{kf}{2} = \frac{f\omega}{2c} \quad . \tag{2b}$$

The electric field component E_{η} , roughly in the acceleration

direction along the z-axis, is

$$E_\eta = -\frac{i}{h}\sqrt{\frac{1}{\xi^2-\eta^2}}\ \frac{\partial}{\partial\xi}\sqrt{\xi^2-1}\ B_\phi \quad ; \tag{2c}$$

The field component E_ξ , roughly perpendicular to the z-axis, is

$$E_\xi = \frac{i}{h}\sqrt{\frac{1}{\xi^2-\eta^2}}\ \frac{\partial}{\partial\eta}\sqrt{1-\eta^2}\ B_\phi \quad . \tag{2d}$$

These formulas give the exact fields in an ellipsoidal cavity once the frequency, or h , has been determined from the radial boundary condition $E_\eta(\xi_o) = 0$.

The particle trajectory is assumed to be exactly parallel to and to pass through a narrow region about the z-axis $|\eta| \ll 1$, $\xi \simeq 1$. The magnetic field B_ϕ is always exactly perpendicular to the particle direction. However, the electric field components E_η and E_ξ are exactly parallel resp. perpendicular to $\underline{z}$ at $\eta = 0$ only : for $\eta \neq 0$ the E_η field has a small component in the ξ- direction , and vice versa. These components will be ignored to a first approximation; henceforth $E_\parallel = E_\eta$, and $E_\perp = E_\xi$.

The energy transfer in the parallel direction $\Delta p_\parallel$ gives the accelerating energy $\Delta E = c\Delta p_\parallel$, while the momentum transfer in in the perpendicular direction, $\Delta p_\perp$, produces the emittance. The momentum transfers are the integrals over time of Equation 1, evaluated along the particle orbit $z = \frac{f\eta}{2} = ct$, $\xi = 1$:

$$\Delta p_\parallel = -\frac{ie\,E_p\,N_\parallel(\xi)}{\omega}\int d\eta\ e^{-ih\eta}\ \frac{S_{1n}(h,\eta)}{\sqrt{1-\eta^2}} \quad , \tag{3a}$$

$$\Delta p_{\perp,E} = \frac{ie\,E_p\,N_\perp(\xi)}{\omega}\int d\eta\,\frac{e^{-ih\eta}}{\sqrt{1-\eta^2}}\,\frac{\partial}{\partial\eta}\,\frac{S_{1n}(h,\eta)}{\sqrt{1-\eta^2}} \quad , \tag{3b}$$

$$\Delta p_{\perp,B} = -\frac{e\,E_p\,N_B(\xi)}{\omega}\int d\eta\,e^{-ih\eta}\,S_{1n}(h,\eta) \quad . \tag{3c}$$

Here E_p is the peak electric field, and $N_\parallel$, $N_\perp$ and N_B are the normalization constants that connect the three fields: They are

$$N_\parallel(\xi) = N_n\,\frac{\partial}{\partial\xi}\sqrt{\xi^2-1}\;R_{1n}(h,\xi) \quad , \tag{4a}$$

$$N_\perp(\xi) = N_B(\xi) = N_n\,R_{1n}(h,\xi) \quad ; \tag{4b}$$

These formulas all have the same normalizing factor

$$N_n = \left[\frac{S_{1n}(h,\eta)}{\sqrt{1-\eta^2}}\right]^{-1}_{\max,\,\eta}\left[\frac{\partial}{\partial\xi}\sqrt{\xi^2-1}\;R_{1n}(h,\xi)\right]_{\max,\,\xi} \quad , \tag{4c}$$

where $[\,]_{\max,x}$ denotes the maximum of the function in brackets with respect to x . These factors are chosen such that the peak electric field E_p is the single strength parameter.

The Fourier transforms in Equations (3) show various interesting features: there is a 180 degree phase difference between $\Delta p_\parallel$ and $\Delta p_{\perp,E}$, due to the factor $-i$ resp. i , and a 90 degree phase difference with $\Delta p_\perp$. In addition there is an extra phase factor from the initial position $z_o = f\eta_o/2$. Hence the complex exponential $\exp - ih\eta$ becomes $\exp - ih(\eta+\eta_o)$. The phase η_o should be such that the accelerator maximizes $\Delta p_\parallel$. Since

the functions $S_{ln}(h,\eta)$ have a well-defined parity (odd for n even, and vice versa) this maximization demands that

$$-i \exp - ih(\eta+\eta_o) = \cos h\eta$$

when S_{ln} is even in η, and $\sin h\eta$ for S_{ln} odd; what is more, this replacement should be done in each of Equations (3). Let n be odd, for the sake of argument. Then the exponential in (3a) and (3b) becomes $\cos h\eta$, but in (3c) $\sin h\eta$. Now the derivative $\partial/\partial\eta$ in (3b) of an even function changes the parity to odd, hence, the integral will vanish. Likewise, the integral in (3c) is over an even function times an odd factor $\sin h\eta$, and this integral vanishes also.

Not all electrons enter the fields with exactly the correct phase: the momentum transfer for an electron with phase angle η_b will be given by

$$\Delta p_{\parallel}(\eta_b) = |\Delta_m p_{\parallel}| \cos h\eta_b \quad , \tag{5a}$$

$$\Delta p_{\perp,E}(\eta_b) = |\Delta_m p_{\perp,E}| \sin h\eta_b \quad , \tag{5b}$$

$$\Delta p_{\perp,B}(\eta_b) = - |\Delta_m p_{\perp,B}| \sin h\eta_b \quad , \tag{5c}$$

an angle factor times the absolute value of the momentum transfer, i.e. the integrals (3) evaluated with the maximizing phase.

Notice that these considerations pertain only to the field structure along η, and do not depend on the particle distance from the z-axis: Its effect will come in only through the factor $N(\xi)$ in Equation (3).

The integrals in Equation (3) are, to our knowledge, not expressible in closed form except in the limit $h \to \infty$. Then the spheroidal functions S_{ln} becomes

$$S_{ln}(h,\eta) \sim H_{n-1}(\eta\sqrt{h}) \exp - h\eta^2/2 \quad ,$$

and the factor $(1-\eta^2)^{\frac{1}{2}}$ becomes simply unity.

Whence,

$$|\Delta p_{\parallel}| = \frac{eE_p N_{\parallel}(\xi)}{\omega} \sqrt{\frac{2\pi}{h}} H_{n-1}(\sqrt{h}) \exp - h/2 \quad , \qquad (6a)$$

$$|\Delta p_{\perp,E}| = \frac{eE_p N_{\perp}(\xi)}{\omega} h\sqrt{\frac{2\pi}{h}} H_{n-1}(\sqrt{h}) \exp - h/2 \quad , \qquad (6b)$$

and

$$|\Delta p_{\perp,B}| = \frac{eE_p N_{\perp}(\xi)}{\omega} \sqrt{\frac{2\pi}{h}} H_{n-1}(\sqrt{h}) \exp - h/2 \quad ; \qquad (6c)$$

The magnitude of the transverse momentum change is basically proportional to the accelerator's energy gain. A small emittance, therefore, depends crucially on the smallness of the inital phase η_b , and on the transverse bunch size ξ_b through the normalization factors of Equation (4).

Close to the cavity axis, i.e. $\xi \simeq 1$, Equation (4) can be evaluated with the limiting form for the radial eigenfunctions $R_{ln}(h,\xi)$ near $\xi = 1$. These are approximately, for large h ,

$$R_{ln}(h,\xi) \simeq \left(\frac{\pi h}{2}\right)^{\frac{1}{2}} \frac{r}{f} \quad , \qquad (7a)$$

and

$$\frac{\partial}{\partial \xi}\left[\sqrt{\xi^2-1}\ \ R_{1n}(h,\xi)\right] \simeq \left(\frac{\pi h}{2}\right)^{\frac{1}{2}} \quad ; \tag{7b}$$

where the radius $r = \frac{f}{2}\sqrt{\xi^2-1}$.

The maximum in the radial dependence of parallel electric field E_η takes place at the cavity axis, hence

$$\frac{\partial}{\partial \xi}\left[\sqrt{\xi^2-1}\ \ R_{1n}(h,\xi)\right]_{\max,\ \xi} = \left(\frac{\pi h}{2}\right)^{\frac{1}{2}} \quad , \tag{7c}$$

The normalization factors (4) are near the axis:

$$N_{\parallel} = \left[\frac{S_{1n}\ (h,\eta)}{\sqrt{1-\eta^2}}\right]_{\max,\ \eta} \quad , \tag{8a}$$

and

$$N_{\perp} = N_{\parallel}\ \frac{r}{f} \quad . \tag{8b}$$

This gives for Equation 6:

$$\Delta P_{\parallel,E} \simeq \frac{r}{(\lambda/\pi)}\ \Delta P_{\parallel} \quad . \tag{8c}$$

It is satisfying that these results are so obvious; in fact, the equivalent of Equation (8) has already been used to estimate the emittance. The present analysis, therefore, adds the connection with the spheroidal cavity modes, but no new insights. Perpendicular momentum transfer is produced by the magnetic field B_ϕ , but mainly by the perpendicular electron field E_ξ , on account of the additional, large, h in

Equation (6b). Taking only $\Delta p_{\perp,E}$, the perpendicular momentum transfer is for the edge of a small bunch ($hn_b << 1$, $hr_b << 1$)

$$\Delta p_{\perp} = \Delta p_{\parallel} \, 2\pi^2 \, (r_b/\lambda) \, (z_b/\lambda) \quad . \tag{9}$$

The conclusion from Equation (9) is that the electron bunches to be accelerated in the RF cavity should be very small compared to the wavelength both in radius r_b and axially z_b. Typical dimensions would be 1% of a wavelength, in both r and z, for

$$\Delta p_{\perp}/\Delta p_{\parallel} \simeq \frac{1}{500} \quad .$$

Energy Transfer From Cavity Modes To Gaussian-Shaped Relativistic Charge Bunch

The energy transfer from cavity modes to a single particle was calculated earlier. This section computes the energy transfer to a Gaussian bunch of electrons. The bunch is assumed to be narrow in the radial direction, but it has a varying width along the cavity axis.

Two limiting cases are obvious: a bunch that is narrow compared to the axial wavelength of the cavity modes looks like a single particle for energy transfer purposes. On the other hand, a bunch that stretches over a few axial wavelengths gets little energy transfer.

Relativistic motion of the particles precludes any shape changes in the bunch. Therefore, the energy transfer can be calculated by averaging over the particle density in the bunch,

$$n(\zeta) = \frac{N}{\alpha W\sqrt{2\pi}} \exp - \zeta^2/2\alpha^2W^2 : \qquad (10)$$

here N is the number of bunch particles, ζ is the bunch coordinate $\zeta = z - ct$, and α is the bunch width in terms of the waist size

$$w = \frac{\lambda\sqrt{h}}{\pi} = \left(\frac{f\lambda}{\pi}\right)^{1/2} \qquad (11)$$

The energy transfer from cavity mode n to a relativistic particle at a phase angle $s_o = \omega\Delta t = \omega\zeta/c$ with respect to the position of maximum energy transfer, is

$$\Delta E(s_o) = \Delta E_o \cos s_o, \tag{12a}$$

where

$$\Delta E_o = (eE_p \lambda_n) \frac{N_n}{\sqrt{2\pi}} \left(\frac{\pi W}{\lambda}\right) \exp - \frac{1}{2}\left(\frac{\pi W}{\lambda}\right)^2 . \tag{12b}$$

The energy transfer to the Gaussian bunch ΔE_b is then

$$\Delta E_b = \Delta E_o \frac{N}{\alpha W\sqrt{2\pi}} \int d\zeta \cos \frac{2\pi\zeta}{\lambda} \exp - \zeta^2/2\alpha^2W^2, \tag{13a}$$

$$= N\Delta E_o \exp - 2\pi \alpha^2 f/\lambda . \tag{13b}$$

The energy transfer for a bunch is, of course, proportional to the energy transfer per particle to the number of particles, times a shape factor. The shape factor is a Gaussian due to the Gaussian bunch shape: an arbitrary localized bunch will give another shape factor, dependent on the same parameter $2\pi \alpha^2 f/\lambda$. In any case, the energy transfer does not decrease too much for

$$\alpha \lesssim \frac{1}{2}\sqrt{\lambda/\pi f} . \tag{14a}$$

The allowable bunch width αW is therefore

$$\alpha W \lesssim \frac{\lambda}{2\pi} . \tag{14b}$$

This result is very reasonable: a bunch width less than 1/6 of the free space wavelength does not affect the energy transfer. Similar results are obtained in the bunched electron accelerator PHERMEX.

NUMERICAL EVALUATIONS AND CONCLUSIONS

The energy transfer from the exact cavity fields as computed numerically deviated considerably from the value given by the Hermite-Gaussian approximation. An exact formula for the energy transfer is obtained as follows. Consider the differential equation

$$\left[\frac{d}{d\eta}(1-\eta^2)\frac{d}{d\eta} + \lambda_{ln} - h^2\eta^2 - \frac{1}{1-\eta^2}\right] S_{ln}(h,\eta) = 0 \quad , \tag{15}$$

multiply this by

$$T \equiv e^{ih\eta}\Big/\sqrt{1-\eta^2} \quad , \tag{16}$$

and integrate from $\eta = -1$ to $\eta = 1$.

Integration by parts gives

$$\left[T'(1-\eta^2)S_{ln} - T(1-\eta^2)\,S'_{ln}\right]_{-1}^{1} =$$

$$\int_{-1}^{1} S_{ln}\left[\frac{d}{d\eta}(1-\eta^2)\frac{d}{d\eta} + \lambda_{ln} - h^2\eta^2 - \frac{1}{1-\eta^2}\right] T\, d\eta \quad . \tag{17}$$

The bracketed operator working on T simplifies considerably;

$$\left[\ \right]T = (1-\eta^2)^{-\frac{1}{2}}(\lambda_{ln}-h^2)\, e^{ih\eta} \quad . \tag{18}$$

Therefore, the energy transfer integral is

$$\int_{-1}^{1} \frac{S_{1n}(h,\eta)\ e^{ih\eta}}{\sqrt{1-\eta^2}}\ d\eta \quad = \quad \frac{\left[(1-\eta^2)(T'S-TS')\right]_{-1}^{1}}{\lambda_{1n}-h^2} \quad . \qquad (19)$$

The term in square brackets should be evaluated in the limit $|\eta| \to 1$; In this limit the function S_{1n} is

$$S_{1n}(h,\eta) \simeq N_{1n}(1-\eta^2)^{\frac{1}{2}}\ k_3 h/2 \qquad , \qquad (20)$$

where k_3 for large h is found as (Slepian 1965)

$$k_3 = e^{-h}\ h^{n/2}\ 2^{(3n-1)/2}\sqrt{\pi} \quad , \qquad (21)$$

and the normalization factor N_{1n} is such that the maximum of S_{1n} is approximately unity:

$$N_{1n} \simeq \sqrt{(n-1)!\ \pi/2} \quad . \qquad (22)$$

The square brackets in (19), exclusive of the sinusoidal term, then become simply $N_n\ k_3\ h$. The energy transfer integral becomes, approximately,

$$U \simeq \pi\sqrt{(n-1)!}\ h^{(n+s)/2}\ 2^{3n/2}\ e^{-h}\ \begin{matrix}\sin\\ \cos\end{matrix}\ h\ /(\lambda_{1n}-h^2) \quad : \qquad (23)$$

(the sin-function should be chosen for n even, cos- for n odd).

This result should be used with caution, because the estimate for the maximum value of S_{1n} contains an additional constant of order unity.

Moreover, the above formulas use only the first terms in the asymptotic expansions. Figures 1-3 show some numerical results.

The frequency h as determined from the WKB-approximation to the radial spheroidal wave function is given in Figure 1: In Figure 1(a) the axial mode number $n = 1$, and the radial mode number parametrizing the curves varies from $\ell = 1$ to $\ell = 21$. The data are in general agreement with the analytical estimate $h \sim (\xi_o^2-1)^{-\frac{1}{2}} (j'_\ell+\ldots)$. Figure 1(b) given the frequency but for $n = 4$; The frequency is higher as expected. The frequencies are in good agreement with those found by using the exact radial spheroidal wavefunction R_{ln}.

Figure 2 gives the parallel, and Figure 3 the perpendicular energy transfer, Equation (6), for $1 \leq n \leq 5$ as function of the cavity position ξ_o and parametrized by the radial mode number ℓ. Here the energy transfer is evaluated with Hermite-Gaussian approximation: Figure 2(a) for $n = 1$ shows an energy transfer that increases *linearly with* ξ_o; the transfer is very small for large ℓ, and appreciable for $\ell = 1$ only.

For $n = 4$, as in Figure 2(b), the story is different: Now the energy transfer is good for $\ell = 1$ and $\xi \geq \sqrt{2}$ or so, and for larger ℓ the transfer increases, again linearly with ξ_o, to reasonable values.

Figure 2(c) compares these data, obtained from the Hermite-Gaussian approximation, with the exact formula (19) evaluated numerically. Only data for a confocal cavity $\xi_o = \sqrt{2}$ are available at this moment: the figure shows $\Delta E_\parallel / eE_p \lambda$ as function of axial mode number n, parametrized by ℓ. The surprise here is that the agreement is not uniformly good: what is worse, the values from the Hermite-Gaussian approximation are too high, by a large factor.

Probable causes for this discrepancy are under investigation: one possibility is indicated by the exponential factor $\exp(-h)$ in Equation (23), versus $\exp(-h/2)$ in Equation (6), for $h \approx 10$ a factor of order 100 . The difference in exponential decay with h reflects the unfortunate fact that the Hermite-Gaussian approximation is not good in its "tails"; the axial spheroidal function falls off more rapidly as h increases.

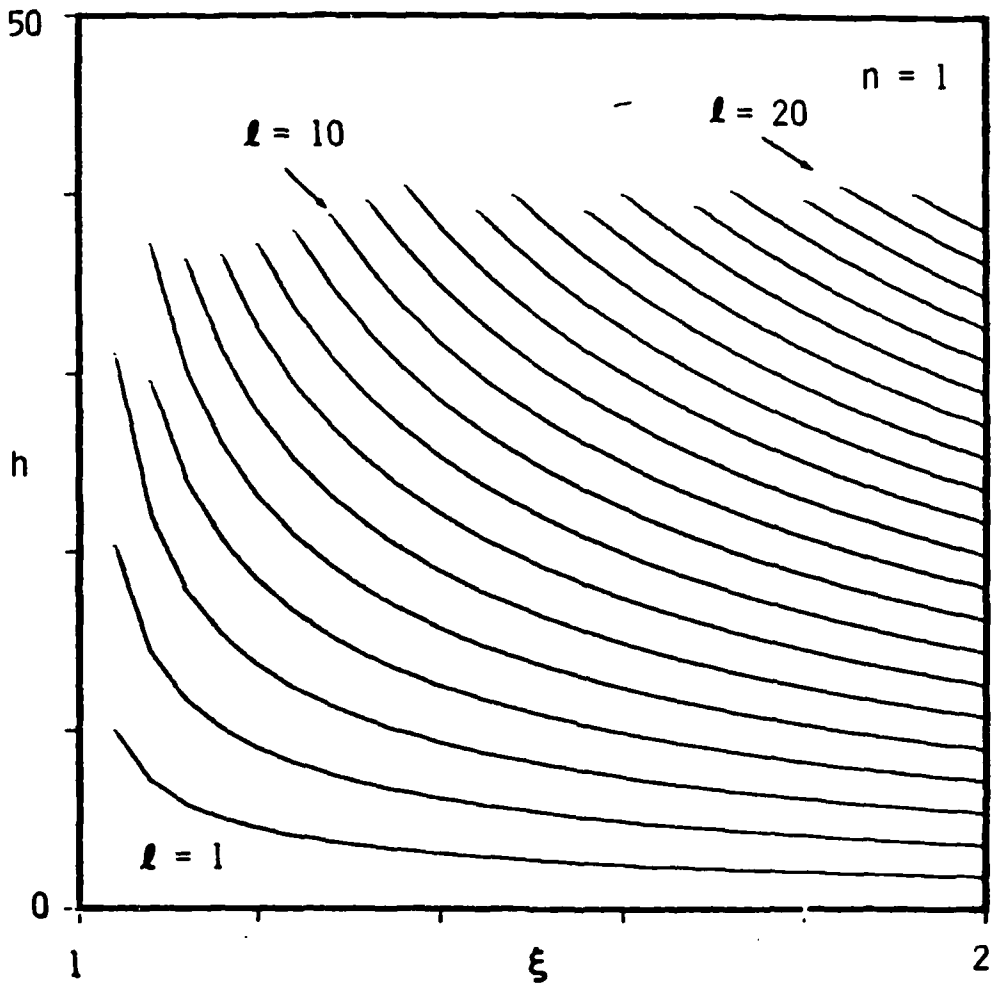

Figure 1a

The frequency $h = \frac{f\omega}{2c}$ as function of wall position ξ_0 for axial mode number $n = 1$.

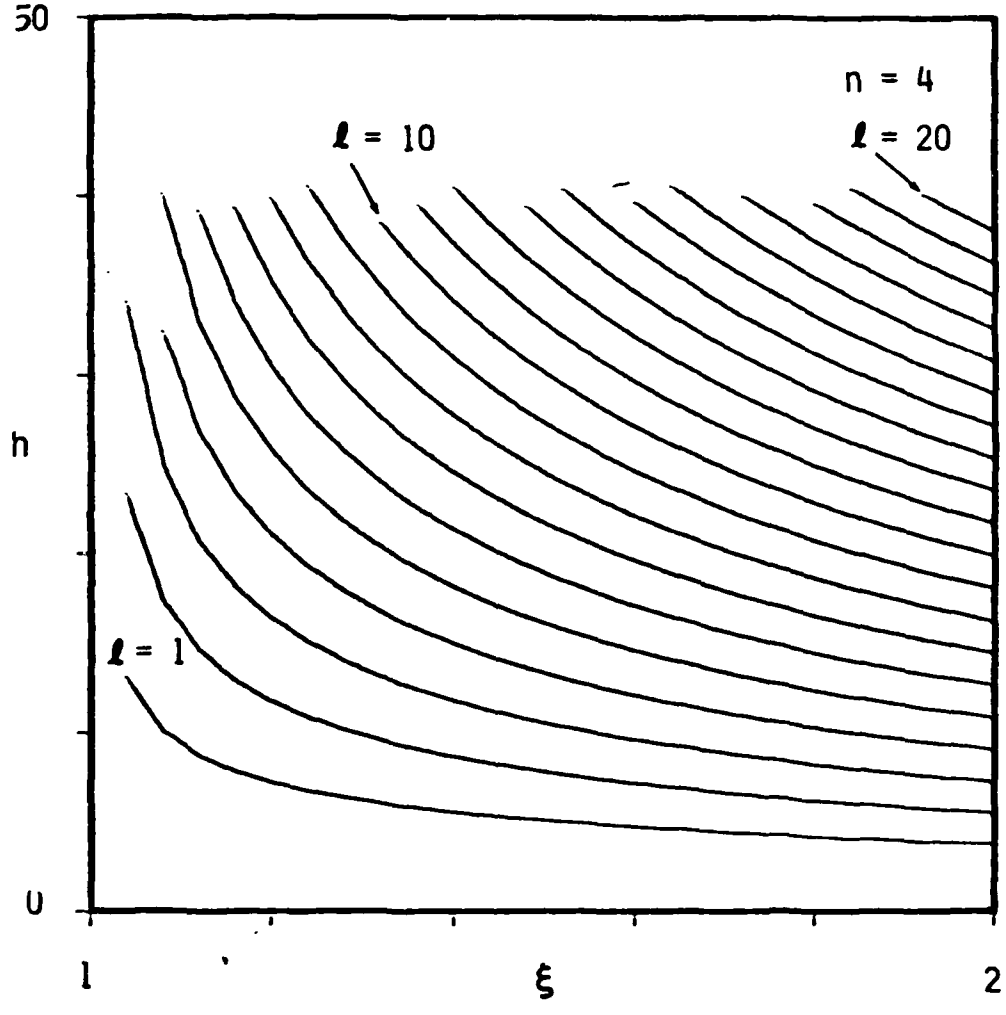

Figure 1b

The frequency $h = \frac{f\omega}{2C}$ as function of wall position ξ_0 for axial mode number $n = 4$.

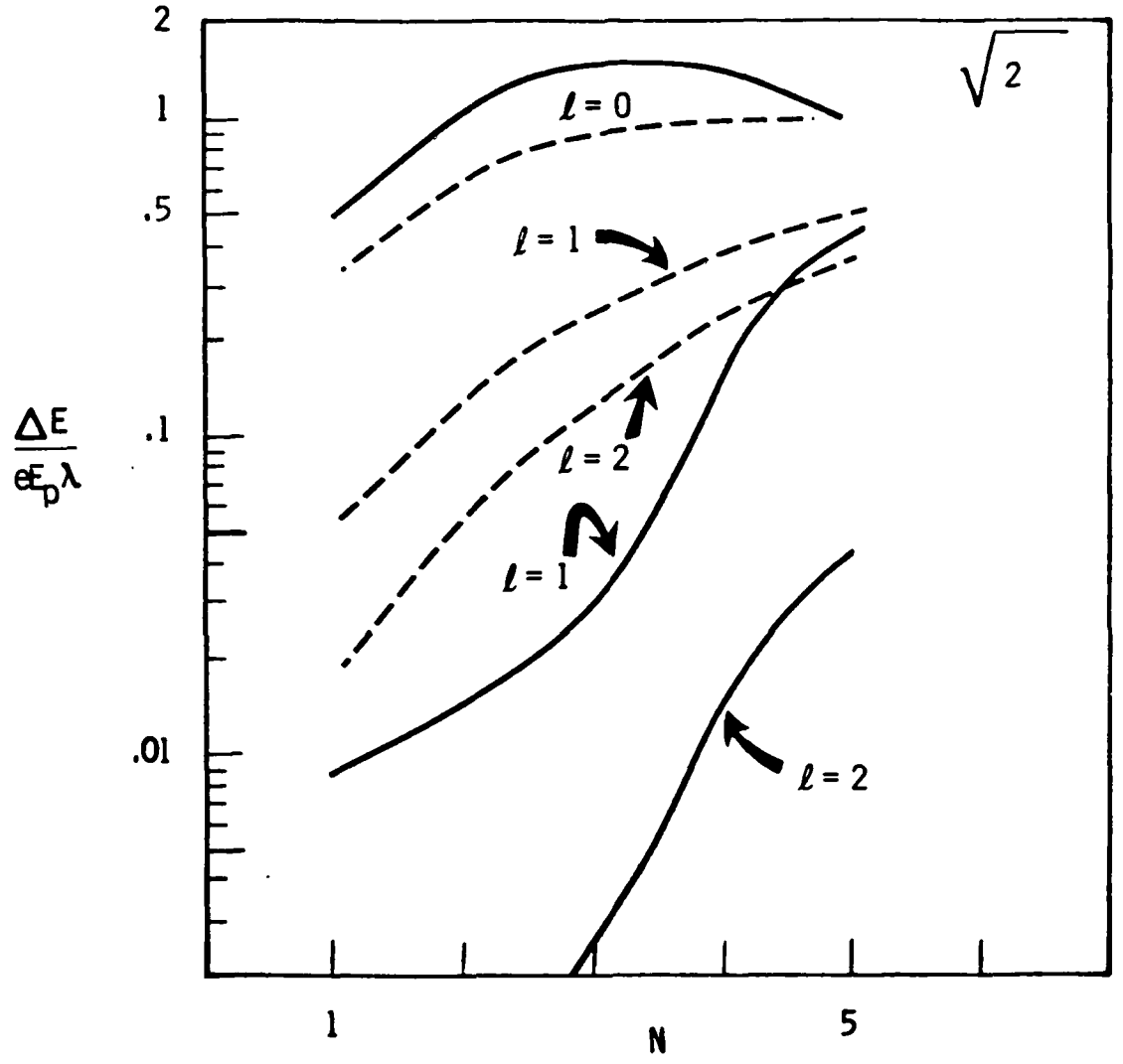
2
1
.5
.1
.01
$\frac{\Delta E}{eE_p\lambda}$
$\sqrt{2}$
$\ell = 0$
$\ell = 1$
$\ell = 2$
$\ell = 1$
$\ell = 2$
1
N
5

APPENDIX V

MISCELLANEOUS ON SPHEROIDAL FUNCTIONS

The properties of the spheroidal functions are less known that those of the more common special functions. In this section various useful formulas are given, asymptotic expansions are verified, etc.

Particularly useful sources are Meixner and Schafke (Reference 1), and Flammer (Reference 2). Numerical data, and the computer code used by us, were obtained by courtesy of Dr. A. L. Van Buren, NRL (References 3 and 4).

Normalization

There are various normalizations in use. The one adopted by some modern writers is Meixner's:

$$\int_{-1}^{1} \left[S_{mn}(h,\eta) \right]^2 d\eta = \frac{2}{2n+1} \frac{(n+m)!}{(n-m)!} .$$

This is equivalent to

$$S_{mn}(o,\eta) = P_n^m(\eta) ,$$

where P is a Legendre polynomial. The set S_{mn} is complete:

$$f(x) = \sum_{n=m}^{\infty} \frac{2n+1}{2} \frac{(n-m)!}{(n+m)!} \int dt\, f(t)\, S_{mn}(h,t)\, S_{mn}(h,x)$$

In this report we do not use any of the standard normalization: instead, the function that gives the electric field is normalized to unity at its maximum.

APPROXIMATION FOR RADIAL FUNCTION

The approximation for the radial function $R_{mn}(h,\xi)$ is (Reference 1, Section 3.91)

$$(\xi^2-1)^{\frac{1}{2}} R_{mn}(h,\xi) \simeq \left(\frac{\pi}{2h}\right)^{\frac{1}{2}} \left(\frac{s}{s'}\right)^{\frac{1}{2}} J_m(s) \quad , \tag{1}$$

where

$$s = h\sqrt{\xi^2-1} - \frac{q}{2} \arccos \xi^{-1} - \frac{q^2+3}{16h\xi^2}\sqrt{\xi^2-1} + \ldots \quad . \tag{2}$$

Near the axis $\xi-1$

$$R_{mn}(h,\xi\simeq 1) = \left(\frac{\pi}{2h}\right)^{\frac{1}{2}} \frac{1}{m!} \left(\frac{h}{2}\right)^m (\xi^2-1)^{m/2} \times \left[1 - \frac{q}{2h} - \frac{q^2+3}{16\gamma^2} + \ldots\right]^m \quad .$$

Here $q = 2n-2m+1$.

The following figure gives a comparison between $(\xi^2-1)^{\frac{1}{2}} R_{1n}$ and its approximation. For frequencies h of interest $h \geq 10$, the argument is extremely close. The figure shows a worst case, $h = 10$ and $n = 5$. The "exact" curve is the left side of Equation (1), the curve marked "appr" is the right side, with s from Equation (2). The dashed curve is the approximation (1), but neglecting the last term in s . Each function is normalized to the maximum.

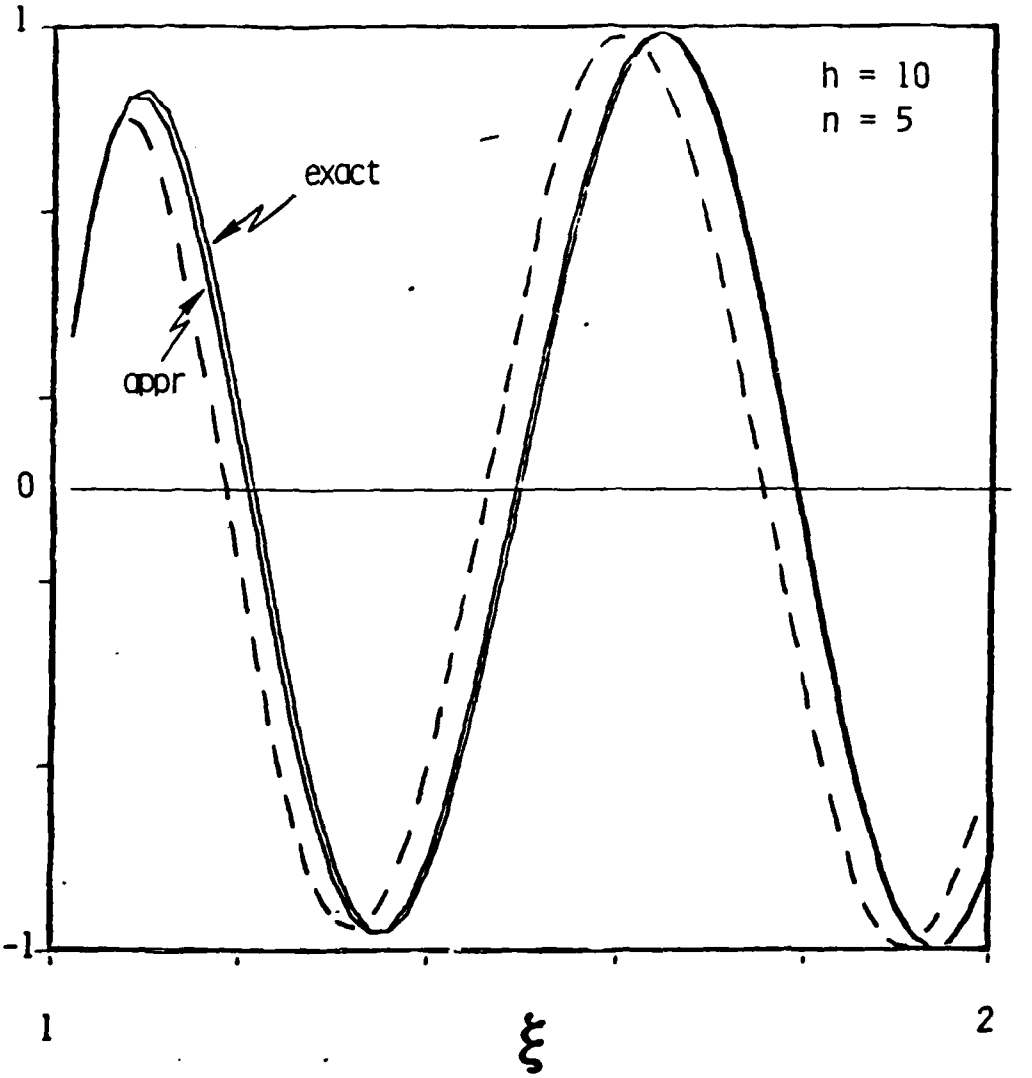

Comparison Between Exact and Approximate Radial Spheroidal Wave Function

ASYMPTOTICS FOR AXIAL FUNCTION

The asymptotic expansion for large frequency $h \to \infty$ for the angular function $S_{mn}(h,\eta)$ is:

$$(1-\eta^2)^{-\frac{1}{2}} S_{mn}(h,\eta) \simeq H_{n-m}(\eta\sqrt{h}) \exp - h\eta^2/2 \quad ,$$

$$= \sum_{r=-\infty}^{\infty} a_r^{\ell} H_r(\eta\sqrt{h}) \exp - h\eta^2/2 \quad ,$$

where $\ell = n-m$,

and the coefficients a_r^{ℓ} satisfy a five-term recursion system given e.g. in Reference 2, Section 8. The formulas are fairly unwieldy: The following figure is a comparison between $(1-\eta^2)^{-\frac{1}{2}} S_{1n}(h,\eta)$ and $H_{n-1}(\eta\sqrt{h}) \exp - h\eta^2/2$ for two values $h = 10$ and 20 , and two values $n = 2$ and 4 .

The approximation is satisfactory for $h = 20$ and both values of n ; although there are clear deviations for $n = 5$. For lower frequency $h = 10$ the agreement is acceptable for $n = 2$, but bad for $n = 5$. Slepian (Ref. 5) gives a more complete treatment of the asymptotics in spheroidal functions which, however, is fairly complicated. The relation above should be reasonably good in the region $|\eta| \leq h^{-\frac{1}{2}}$, but no in the Gaussian "tails" where $\eta\sqrt{h} >> 1$.

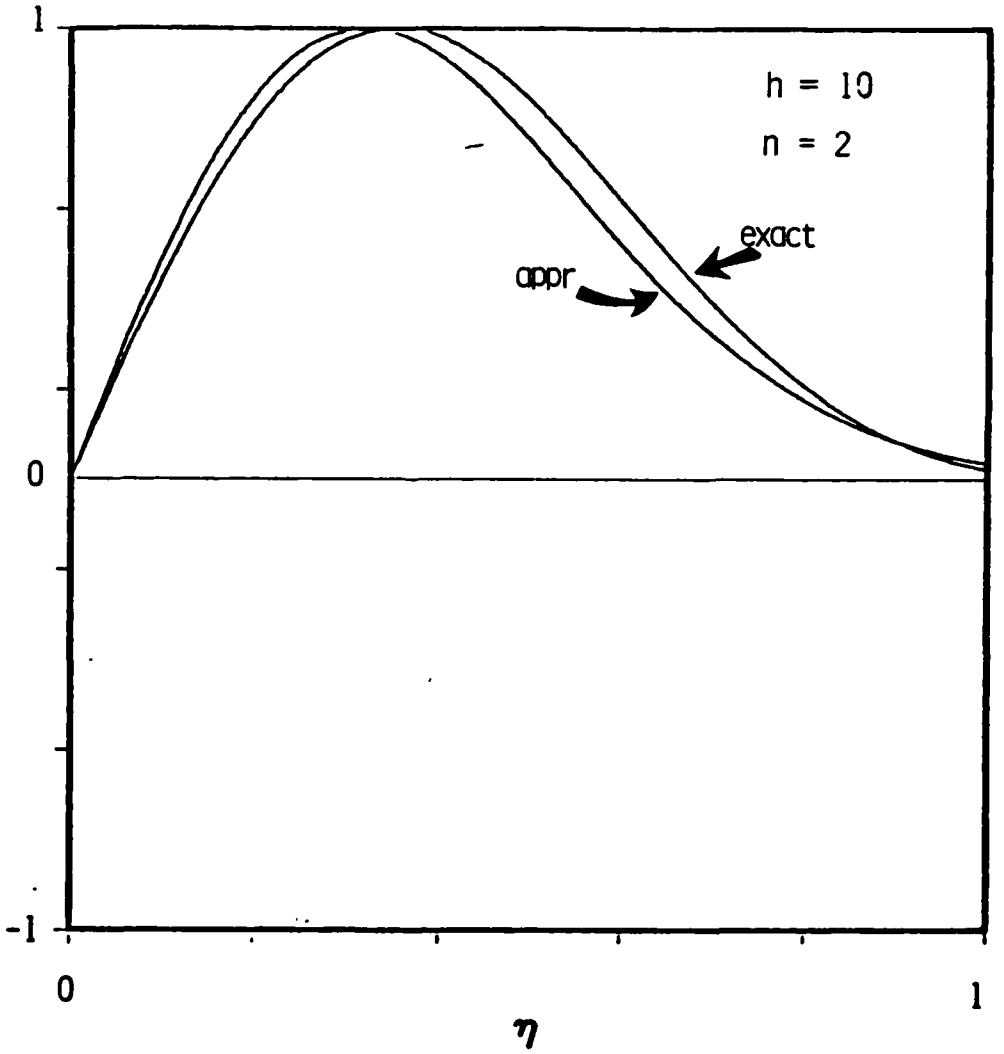

Comparison Between Exact and Approximate Axial Spheroidal Wave Function for: h = 10 n = 2

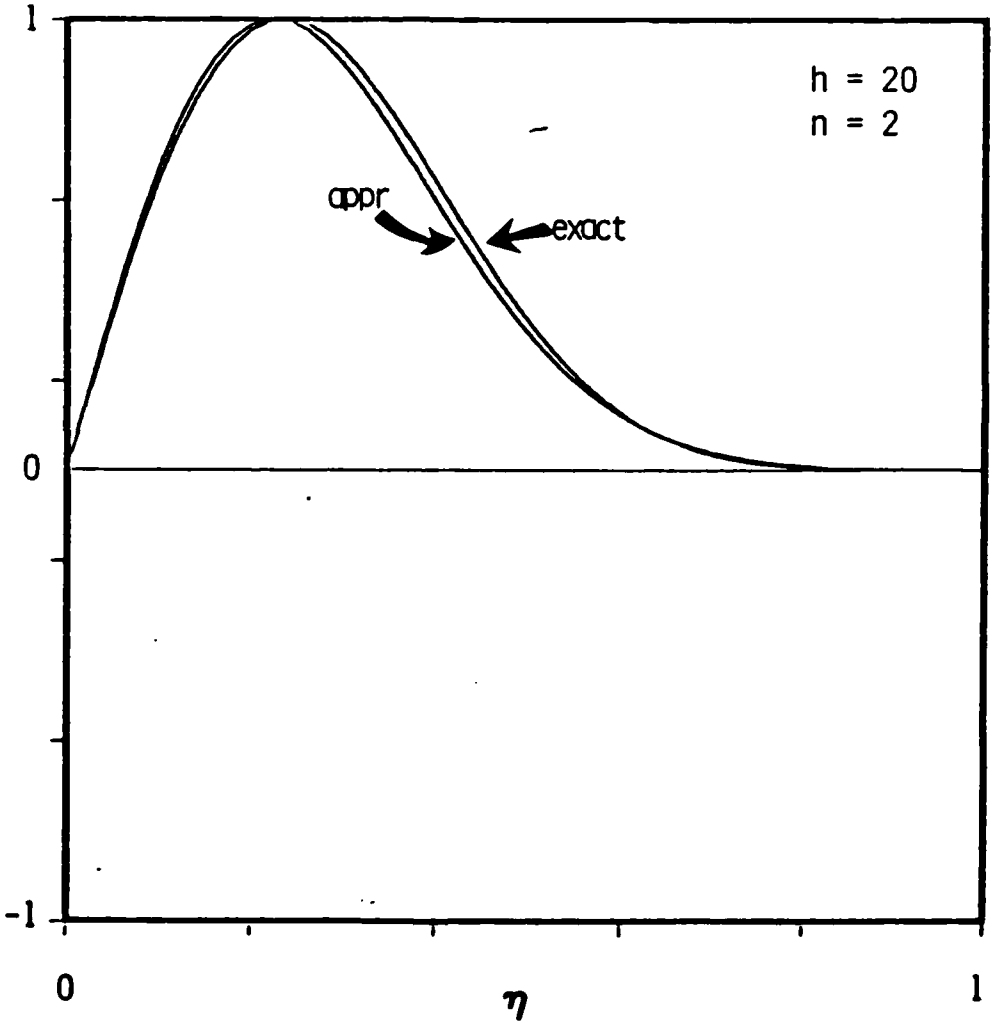

Comparison Between Exact and Approximate Axial Spheroidal Wave Function for: h = 20 n = 2

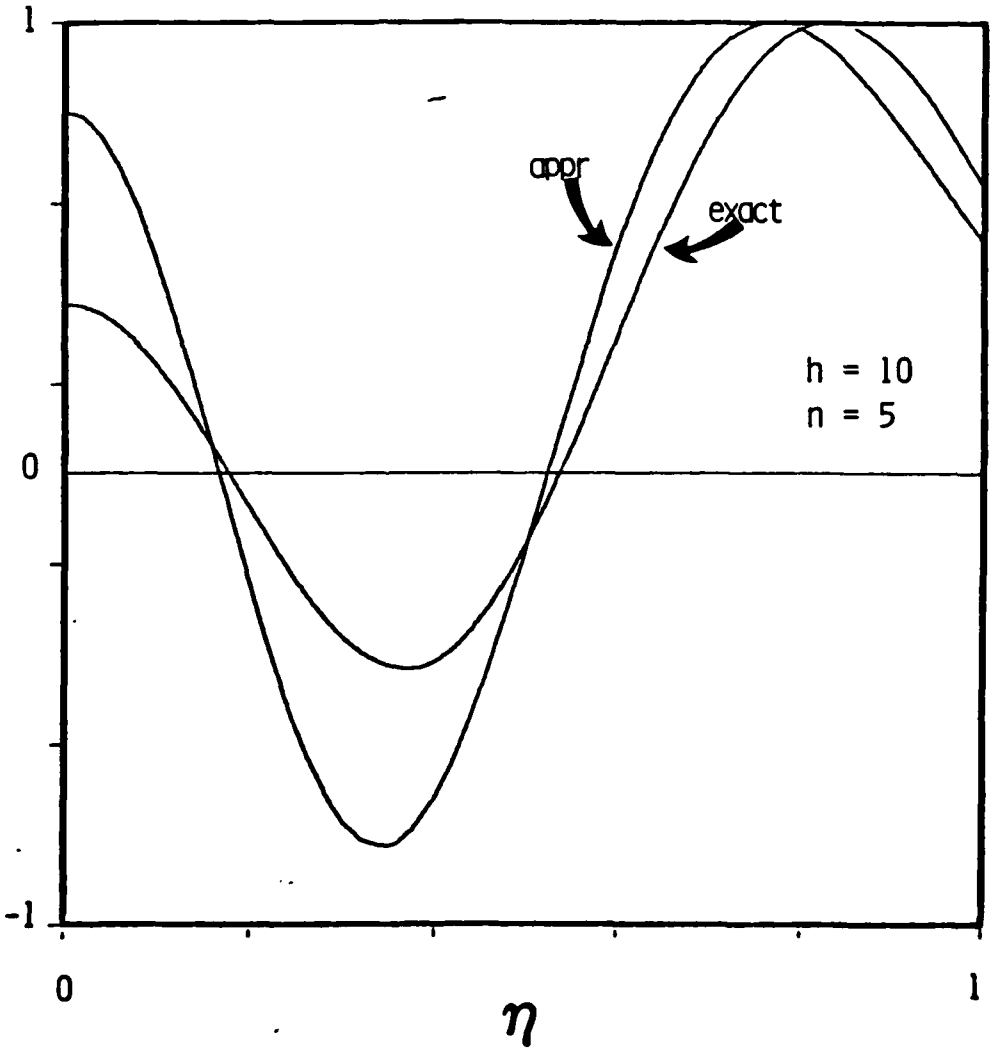

Comparison Between Exact and Approximate Axial Spheroidal Wave Function for: h = 10 n = 5

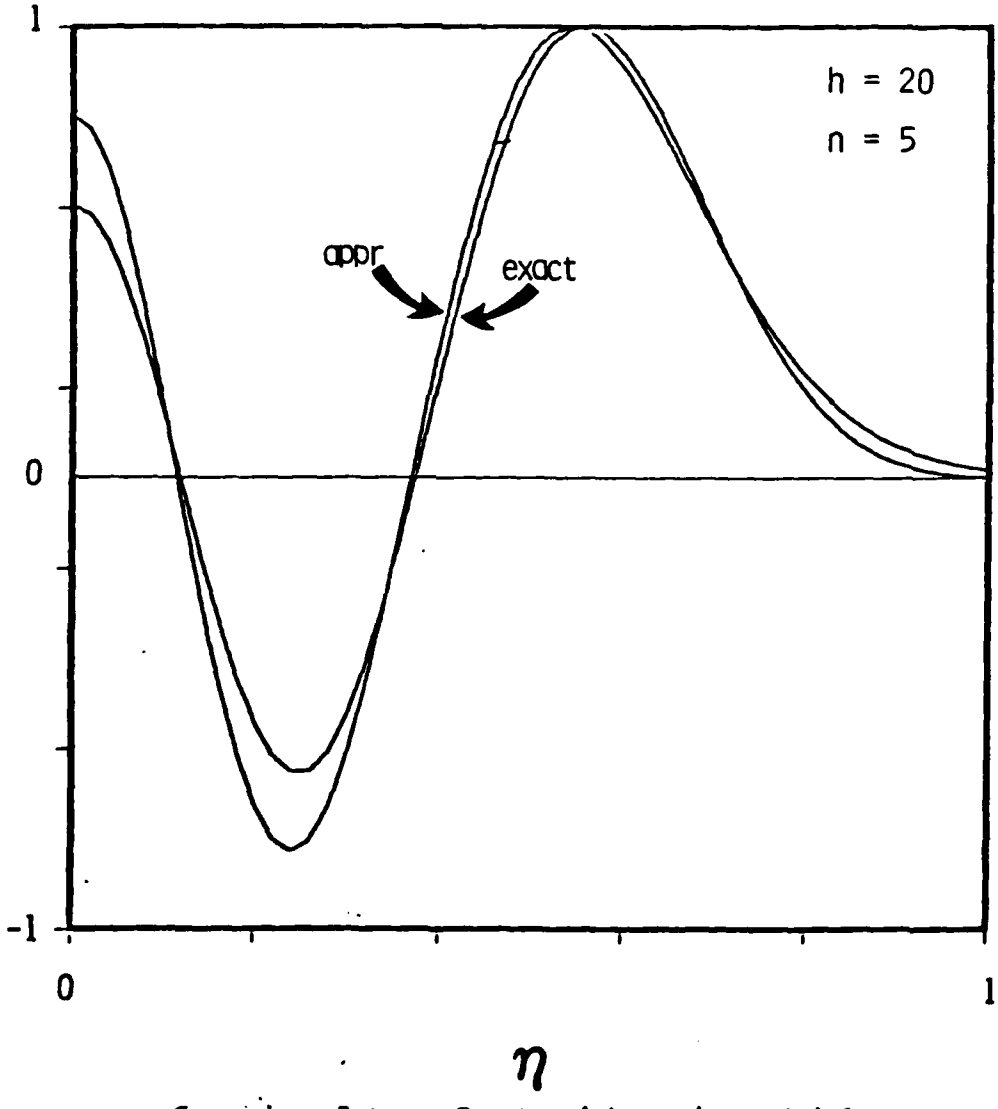

Comparison Between Exact and Approximate Axial Spheroidal Wave Function for: h = 20 n = 5

WKB Approximation for Axial Spheroidal Function

Quite often the WKB approximation is very reliable, especially for the higher mode envisioned in the transverse RF accelerator. To our knowledge, however, this approxmation has not been derived before for the spheroidal functions. Consider the function

$$u_n(h,\eta) = \sqrt{1-\eta^2}\, S_{in}(h,\eta) \quad ; \tag{1}$$

it satisfies the Schroedinger equation

$$u'' = Q(\lambda,\eta)u \quad , \tag{2a}$$

where

$$Q = \frac{h^2\eta^2-\lambda}{1-\eta^2} \quad ; \tag{2b}$$

λ is the eigenvalue for the spheroidal function, and h is the frequency $h = f\omega/2c$.

The WKB-approximation in the region between the turning points $\eta_t = \sqrt{\lambda}/h$ is

$$u \simeq 2(-Q)^{-\frac{1}{4}} \sin\left[\int_{\eta}^{\eta_t}\sqrt{-Q}\, dt + \pi/4\right] \quad . \tag{3}$$

The integral can be done exactly in terms of incomplete Elliptic integrals. Define the argument

$$A = \int\left[\frac{1-\eta^2/\eta_t^2}{1-\eta^2}\right]^{-\frac{1}{2}} \quad . \tag{4}$$

Setting $\eta = \sin\theta$, the integral becomes

$$A = \int_{\theta}^{\theta_t} \sqrt{1-\eta_t^{-2}\sin^2\theta}\, d\theta$$

$$= \sqrt{\lambda}\left[E(\theta_t,\eta_t^{-1}) - E(\theta,\eta_t^{-1})\right] \quad , \qquad (5)$$

where $\theta_t = \text{arc sin } \eta_t$.

The symbol E is the incomplete Elliptic integral, defined by

$$E(\theta,k) = \int \sqrt{1-k^2\sin^2\theta}\, d\theta \qquad (6)$$

Notice that in Equation (5) the parameter η_t^{-1} is greater than unity. Existing tables are typically for parameter less than unity. For computations, therefore, it may be necessary to use the formula (AS 17.4.16)

$$E(U|\eta_t^{-2}) = \eta_t^{-1}\, E(U\eta_t^{-2},\eta_t^{2}) - (\eta_t^{-2}-1)U \quad ,$$

where

$$E(U|m) = \int_0^x \sqrt{\frac{1-mt^2}{1-t^2}}\, dt$$

and $x = \text{sn } U$. Alternatively, the integral can be evaluated numerically as it is needed.

The approximation for the spheroidal function S_{1n} becomes, between the turning points

$$S_{1n}(h,\eta) \simeq \lambda^{-\frac{1}{4}}\left[(1-\eta^2)(1-\eta^2/\eta_t^2)\right]^{-\frac{1}{4}} \sin(\sqrt{\lambda}A(\eta)+\pi/4) \quad , \qquad (7)$$

while the approximation for the derivative of $\sqrt{1-\eta^2}\, S_{1n}$ is

$$\frac{d}{d\eta}\left[\sqrt{1-\eta^2}\, S_{1n}(h,\eta)\right] \simeq \lambda^{\frac{1}{4}}\left[\frac{1-\eta^2/\eta_t^2}{1-\eta^2}\right]^{\frac{1}{4}} \cos(\sqrt{\lambda}\, A+\pi/4) \quad . \tag{8}$$

In the intermediate region about the turning points, where the "potential" is linear with slope $\frac{2\sqrt{\lambda}}{1-\lambda/h^2}$ the approximation is in terms of Airy functions: with

$$S_{1n}(h,\eta) \simeq (1-\eta^2)^{-\frac{1}{2}}\, 2^{5/6}\pi^{\frac{1}{2}}\, \lambda^{-1/12}(1-\lambda/h^2)^{1/6}$$

$$\mathrm{Ai}\left[\left(\frac{2\sqrt{\lambda}}{1-\lambda/h^2}\right)^{1/3}(\eta-\eta_t)\right] \quad . \tag{9}$$

In the region outside the turning points η_t the appropriate formula is similar to (3):

$$u \simeq Q^{-\frac{1}{4}} \exp -\int_{\eta_t}^{\eta} \sqrt{Q}\, d\eta \quad . \tag{10}$$

The integral now becomes

$$\int_{\eta_t}^{\eta} \sqrt{Q}\, d\eta = \sqrt{\lambda}\int_{\theta_t}^{\theta} d\theta \sqrt{\eta_t^{-2}\sin^2\theta - 1} \quad ; \tag{11}$$

it can also be written in terms of incomplete elliptic integrals, but that will not be done here. Instead, direct numerical integration will be used when necessary.

Even without exact evaluation of (11) some observations can be made about the decay rate of S_{1n} for η for outside the turning point, η_t, provided $\eta_t << 1$. This is the case in which the

Gaussian-Hermite approximation applies best. A comparison between the two approximations should be revealing, especially because the functions occur in the energy transfer efficiency. Slepian (Ref. 5) has a third approximation, different from the Gaussian-Hermite, in the region $|\eta| \geq h^{-\frac{1}{2}}$; this approximation should agree closely to the WKB expressions.

REFERENCES:

1. J. Meixner and F. M. Schafke, "Mathematischen Funktionen and Spharoidfunktionen", Springer, 1954.

2. C. Flammer, "Spheroidal Wave Functions", Stanford, 1957.

3. S. Hanish, et. al., "Radial Spheroidal Wave Functions", Volume I, NRL Report 7088, 1970.

4. A. L. Van Buren, et. al., "Tables of Angular Spheroidal Wave Functions", Volume I, NRL, 1975.

5. D. Slepian, "Some Asymptotic Expansions for Prolate Spheroidal Wave Functions", J. Math. and Phys. 44 99 (1965).

APPENDIX VI

MISCELLANEOUS ON DEVICE PHYSICS

Current Limitation Revisited

Maxwell's equations allow a simple estimate for the loading of the accelerator cavity by the beam current. Consider the equation

$$\nabla \times \underline{B} = \mu_o \underline{j} + \frac{1}{c^2} \frac{\partial \underline{E}}{\partial t} \quad : \qquad (1)$$

The free cavity modes calculated earlier in terms of prolate spherical functions follow from (1) by setting the term $\mu_o \underline{j}$ to zero. If $\mu_o \underline{j}$ were everywhere smaller than $c^{-2}\, \partial \underline{E} / \partial t$, or to its equivalent $\nabla \times \underline{B}$, the presence of the beam would scarcely influence the wave fields. Let us compare these terms in an approximate fashion.

The electric field vector is in the same direction as the current density. It is clearly negligible if

$$\text{If} \quad \mu_o |\underline{j}| \ll \frac{\omega E}{c^2} \qquad (2)$$

Numerically, this means

$$j \ll 10^4 \text{ A/cm}^2 \qquad (3)$$

for an accelerator field $E \simeq 10^8$ V/m and frequency $\nu = \frac{\omega}{2\pi} \simeq$ 10Ghz. The constant current density can be spread out about the axis over an area that depends on on the acceptable perpendicular momentum transfer, or emittance. Typically, the beam electron can be a distance $\lambda/20$ from the axis. Therefore, the current I is limited by

$$I \ll \frac{E}{60\mu_o \nu} \simeq 10^2 A \qquad (3)$$

for the given parameters. This current is rather small, however, for a field $E \simeq 10^9$ V/m and $\nu =$ 1Ghz the current limit already 10^4A, and currents $\simeq 10^3$A should be attainable with no problems.

Estimates of this type have been done previously, but based on energy considerations, with the same results.

APPENDIX VII

DIFFRACTION EFFECT ON MODE STRUCTURE

An integral equation for the spheroidal wave function is (Flammer, 5.3.12)

$$2\, S_{1n}(h,\eta)\, R_{1n}(h,\xi) = i^{1-n} \int_{-1}^{1} ds\, e^{ih\xi\eta s} \times J_1\left(h\sqrt{\xi^2-1}\sqrt{1-\eta^2}\sqrt{1-s^2}\right) S_{1n}(h,s) \quad . \qquad (1)$$

Diffraction due to open cavity ends can be calculated approximately in such an integral relation by changing the integration limits from $(-1,1)$ to $(-\eta_o,\eta_o)$, where η_o defines how large the cavity hole is.

Equation (1) for S_{1n} can be simplified considerably by taking a partial derivative $\partial/\partial\xi$, and setting $\xi = 1$. This yields first

$$2\, S_{1n} \frac{\partial R_{1n}}{\partial \xi} = i^{1-n} \int_{-1}^{1} ds\, e^{ih\xi\eta s} \left(ih\eta s\, J_1 + \frac{\xi}{\sqrt{\xi^2-1}}\, h\sqrt{1-\eta^2}\sqrt{1-s^2}\, J_1' \right) S_{1n}(h,s) \; ; \qquad (2)$$

After multiplying by $\sqrt{\xi^2-1}$ the limit $\xi \to 1$ can be taken, with the result

$$\lim_{\xi \to 1}\left[\sqrt{\xi^2-1}\, \frac{\partial R_{1n}}{\partial \xi}\right] S_{1n}(h,\eta) = i^{1-n} \int_{-1}^{1} ds\, e^{ih\eta s}\, \frac{h}{2}\sqrt{1-\eta^2}\sqrt{1-s^2} \times S_{1n}(h,s) \; . \qquad (3)$$

Note that the limit on the left is nonzero.

This formula can be written in different ways. An extra factor $\sqrt{1-\eta^2}$ gives

$$i^{n-1} A_n U_n(h,\eta) = (1-\eta^2) \int_{-1}^{1} ds\, e^{ih\eta s} U_n(h,s) \quad , \tag{4}$$

where

$$U_n(h,\eta) = \sqrt{1-\eta^2}\, S_{1n}(h,\eta) \quad , \tag{5a}$$

and

$$A_n = \lim_{\xi \to 1} \left[\sqrt{\xi^2-1}\, \frac{\partial R_{1n}}{\partial \xi} \right] \frac{2}{h} \quad . \tag{5b}$$

Comparing Equation (4) to the well-known analogue for the zero order spheroidal function

$$2i^{n} R_{on}(h,1)\, S_{on}(h,\eta) = \int_{-1}^{1} e^{ih\eta s} S_{on}(h,s)\, ds \tag{7}$$

we note an extra factor $(1-\eta^2)$. In addition the eigenfunction is not a purely spheroidal function, but has an extra factor $\sqrt{1-\eta^2}$, to make it the potential for the normal electric field

$$E_\xi \propto \frac{\partial U_n(h,\eta)}{\partial \eta} \quad . \tag{8}$$

The interpretation of Equation (4) is then that the normal electric field pattern on the cavity wall is reflected with the propagator $(1-\eta^2) \exp ih\eta s$.

Other forms of Equation (4) are:

$$i^{n-1} A_n S_{1n}(h,\eta) = \sqrt{1-\eta^2} \int_{-1}^{1} ds\, e^{ih\eta s} \sqrt{1-s^2}\, S_{1n}(h,s)\, ds \quad , \quad (9)$$

which would propagate the ϕ-component of the magnetic field, or

$$i^{n-1} A_n V_n(h,\eta) = \sqrt{\frac{1-\eta^2}{\xi_o^2-\eta^2}} \int_{-1}^{1} ds\, e^{ih\eta s} \sqrt{(1-s^2)(\xi_o^2-s^2)}\, V_n(h,s) \quad . \quad (10)$$

where

$$V_n(h,\eta) = \frac{S_{1n}(h,\eta)}{\sqrt{\xi_o^2-\eta^2}} \quad ; \quad (11)$$

This operator propagates the parallel electric field

$$E_\eta \propto V_n(h,\eta) \quad . \quad (12)$$

Notice that Equation (10) seems to contain the cavity wall position ξ_o explicitly (not only through the frequency h). However, the Equations (4) and (9) show that this is not the case: the explicit ξ_o - dependence is cancelled by the extra ξ_o hidden in $V_n(h,\eta)$ of Equation (11). Since all three integral forms are equivalent any of these can be taken as a basis for perturbation. On additional form can be obtained by setting $\xi_o = 1$ in in (10) and (11):

$$i^{n-1} A_n V_n(h,\eta) = \int_{-1}^{1} ds\, e^{ih\eta s} (1-s^2)\, V(h,s) \quad . \quad (13a)$$

where

$$V_n = \frac{S_{1n}(h,\eta)}{\sqrt{1-\eta^2}} \quad (13b)$$

Diffraction effects on the cavity fields are calculated most conveniently with Equation (9), by changing the integration limits from $(-1,1)$ to $(-\eta_o,\eta_o)$. The wave structure in the open cavity $X(h,\eta)$ is now the eigenfunction of

$$i^{n-1} B\, X(h,\eta) = \sqrt{1-\eta^2} \int_{-\eta_o}^{\eta_o} ds\, e^{ih\eta s} \sqrt{1-s^2}\, X(h,s) \quad , \qquad (14)$$

where $B = B_n(\eta_o)$ is the eigenvalue. Notice that B is purely real in the case $\eta_o \longrightarrow 1$, $B = A_n$, and that in this limit

$$X(h,\eta) = X_n(h,\eta;\eta_o) \longrightarrow S_{1n}(h,\eta) \quad ; \qquad (15)$$

Therefore X has the same number of zeroes and symmetry properties as S_{1n} ; even for $n - 1$ even, and vice versa.

For small $\Delta\eta = 1-\eta_a$ the integration in (14) can be approximated by subtracting the average value over the tail ends $(-1,-\eta_o)$ and $(\eta_o,1)$ from the standard integration interval $(-1,1)$ in Equation (9). The result is

$$i^{n-1} B\, X(h,\eta) = \sqrt{1-\eta^2} \int_{-1}^{1} ds\, e^{ih\eta s} \sqrt{1-s^2}\, X(h,s)$$

$$- 2i^{n-1} (\Delta\eta)^{3/2} X(h,\eta_a) \sqrt{1-\eta^2}\, \begin{matrix}\cos\\ \sin\end{matrix}(h\eta\eta_a) \quad . \qquad (16)$$

Here $\cos(h\eta\eta_a)$ applies when $n - 1$ is odd; η_a is a average between 1 and η_o , $\eta_a = (1+\eta)/2$, and $\Delta\eta = 1-\eta_o$.

The perturbation term is proportional to $(\Delta\eta)^{3/2}$, due to the approximation of the square root under the integral. Also, the perturbation has the same symmetry properties as the left side of (16), and the same factor i^{n-1} . Therefore this first order perturbation will not produce an imaginary part in the eigenvalue B .

Following straightforward perturbation theory the unknown function $X(h,\eta)$ can be expanded in a series of spheroidals:

$$X(h,\eta) = \sum_{n=1}^{\infty} a_n S_{1n}(h,\eta) \quad , \tag{17}$$

where the coefficients are given by

$$a_n = \frac{n+\frac{1}{2}}{n(n+1)} \int_{-1}^{1} X(h,\eta)\, S_{1n}(h,\eta)\, d\eta \quad . \tag{18}$$

The constant $(n+\frac{1}{2})/n(n+1)$ is appropriate to the Meixner normalization of the spheroidal functions

$$\int_{-1}^{1} S_{mn}^2 \, d\eta = \frac{(n+m)!}{(n+\frac{1}{2})(n-m)!} \quad . \tag{19}$$

Equation (16) becomes, after interchanging integration and summation, and using the defining integral (9):

$$\sum_{n} (a_n B - a_n A_n + C_n) S_{1n}(h,\eta) = 0 \quad , \tag{20}$$

where

$$c_n = (\Delta\eta)^{3/2}\, X(h,\eta_a)\, \frac{2k+1}{k(k+1)} \int_{-1}^{1} d\eta \sqrt{1-\eta^2}\, \begin{matrix}\cos\\ \sin\end{matrix} h\eta\eta_a\, S_{1n}(h,\eta) \quad . \qquad (21)$$

Evaluation of $X(h,\eta)$ demands another series, but to lowest order

$$X(h,\eta_a) = S_{1n}(h,\eta_a) \quad . \qquad (22)$$

Since the S_{1n}'s are orthogonal there follows

$$a_n = \frac{c_n}{A_n - B} \quad . \qquad (23)$$

The perturbed eigenvalue B is obtained from approximating $X(h,\eta) = X_N(h,\eta;\eta_a)$ in Equation (18) by $S_{1n}(h,\eta)$. Then $a_N = 1$ and

$$B = A_n - c_n \quad . \qquad (24)$$

For practical calculations the coefficients must be evaluated but this is quite tedious. An alternative approach is to solve Equation (9) directly by computer. A suitable algorithm is the interation of Equation (4).

Having found the fields as function of η inside the open cavity, from a perturbation series or by iteration of Equation (14), it is straightforward to calculate the ξ - dependent factor in the fields, $R_{1n}(h,\xi)$. The derivative of Equation (1) with respect to η , an extra multiplication with $\sqrt{1-\eta^2}$, and the limit $\eta \to 1$ yields

$$c_n \frac{R_{1n}(h,\xi)}{\sqrt{\xi^2-1}} = \int_{-1}^{1} ds\, e^{ih\xi s} \sqrt{1-s^2}\, S_{1n}(h,s) \quad , \qquad (25)$$

in complete analogy to Equations (3) and (4). However, now the eigenvalue is

$$C_n = -\frac{4i^{n-1}}{h}\left[\sqrt{1-\eta^2}\ \frac{\partial S}{\partial \eta}\right]_{\lim \eta\to 1}. \tag{26}$$

For an open cavity the ξ-dependent factor $Y_n(h,\xi)$ is now determined by changing the integration limits in (25) from (-1,1) to $(-\eta_o,\eta_o)$.

It is not immediately obvious that this is the correct way to find the ξ-dependence, but this algorithm is certainly reasonable: it makes the field E_z continuous across the focal point η=1, ξ=1. To verify the continuity one should remember that E_z along the axis has two distinct forms,

$$\begin{aligned} E_z &= E_\eta \qquad \text{between foci} \\ E_z &= E_\xi \quad . \quad \textit{outside the foci} \end{aligned} \tag{27}$$

The explicit expressions for E_η and E_ξ evaluated at $\eta = \xi = 1$ then show the continuity at this point.

The field, parallel to the cavity axis, $E_z = E_\eta$, evaluated on the axis $\xi = 1$ between the foci is:

$$E_\eta = -\frac{i}{h}\ \frac{AS_{1n}(h,\eta)}{\sqrt{1-\eta^2}}\left[\frac{\partial}{\partial \xi}\sqrt{\xi^2-1}\ \ R_{1n}(h,\xi)\right]_{\xi=1}. \tag{28}$$

Here A, which depends on the normalization of the various spheroidals is a field strength parameter, whereto we shall return.

Inserting Equation (9), with the explicit value (3b) for its coefficient A_n gives

$$E_\eta(\xi=1,\eta) = -\frac{iA}{4}\left[\frac{\frac{\partial}{\partial\xi}\sqrt{\xi^2-1}\,R_{1n}}{\sqrt{\xi^2-1}\,\frac{\partial}{\partial\xi}R_{1n}}\right]_{\xi\to1} T_n(h,\eta) \tag{29}$$

where

$$T_n(h,\eta) = \int_{-1}^{1} ds\; e^{ihs\eta}\sqrt{1-s^2}\;S_{1n}(h,s) \quad . \tag{30}$$

On the other hand, $E_z = E_\xi$ outside the foci. On the axis $(\eta=1,\xi)$ the field is explicitly

$$E_\xi = \frac{Ai^n}{h}\,\frac{R_{1n}(h,\xi)}{\sqrt{\xi^2-1}}\left[\frac{\partial}{\partial\eta}\sqrt{1-\eta^2}\;S_{1n}(h,\eta)\right]_{\eta\to1} . \tag{31}$$

Use of Equations (25) and (26) for the function R_{1n} gives

$$E_\xi(\xi,\eta=1) = -\frac{Ai^n}{4}\left[\frac{\frac{\partial}{\partial\eta}\sqrt{1-\eta^2}\,S_{1n}}{\sqrt{1-\eta^2}\,\frac{\partial S_{1n}}{\partial\eta}}\right]_{\eta\to1} T_n(h,\xi) \quad . \tag{32}$$

The field E_z is continuous across the focal point $\xi = 1 = \eta$ provided that the constants in the square brackets are equal. This is easily seen directly from the integral relations (9) and (25). Namely, the square brackets do not depend on the normalization constants A_n and C_n, but are simply functionals of $T_n(h,\eta)$ and $T_n(h,\xi)$: and it is clear from definition (30) that

$$T_n(h,\eta \to 1) = T_n(h,\xi \to 1) \quad , \tag{33}$$

Moreover, this equality is true for all derivatives.

Numerical results are shown in Figure 1 and 2. Figure 1 is the field along the z-axis for the case $h = 6$, $n = 2$, η between 0 and 1, and ξ from 1 to 3. The parameter is the size of the cavity opening, parametrized by η_o as indicated. The fields for the closed cavity are concentrated most between the foci, but as the cavity opens up the field pattern widens, and RF leakage increases.

The coupling from RF fields to particles generally deteriorates from opening the cavity. Figure 2 shows the coupling for the case $h = 6$, $n = 2$ as function of cavity hole size η_o, for the lowest three radial modes $\ell = 1$, 2 and 3. The coupling is not affected too much for the lowest mode up to $\eta_o \simeq 0.8$. The higher modes are more sensitive, to the point of reversing the sign of the coupling constant.

The conclusion from the diffraction calculations is that the cavity can be safely opened somewhat, e.g. up to $\eta_o \simeq 0.9$, without too much decrease in the coupling. However, there is no increase in coupling efficiency by increasing leakage from the cavity.

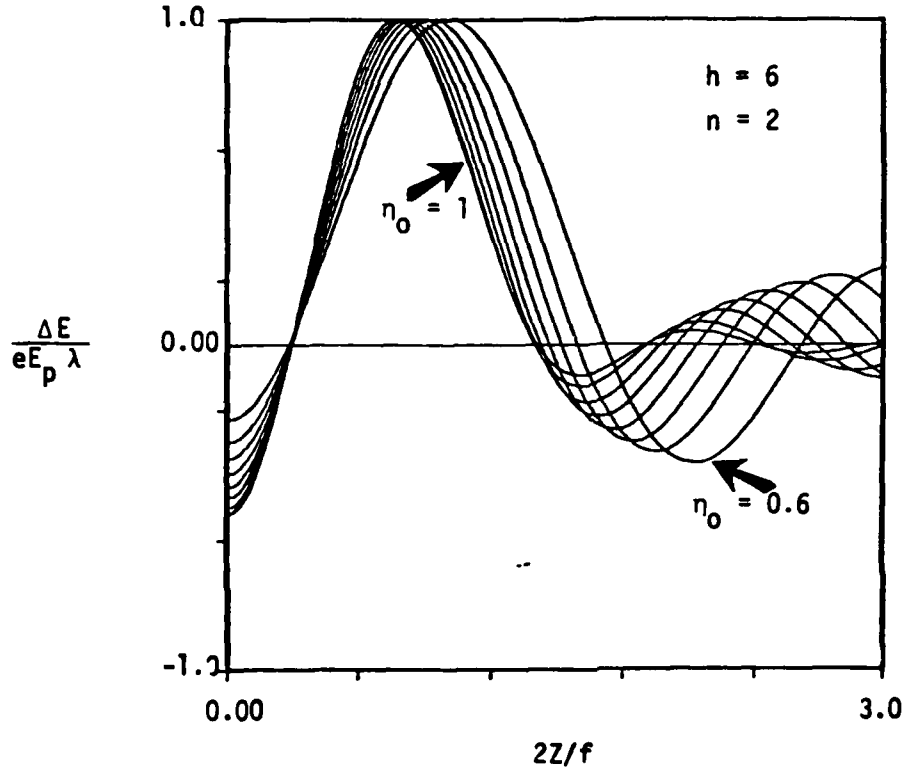

Figure 1. The z-component of the electric field at frequency h = 6, and axial mode number n = 2, along the cavity axis for an open cavity.

The parameter η_o is

$\eta_o = 1 - 0.05\ m$, $m = 0 - 8$ (except $\eta_o = 0.95$).

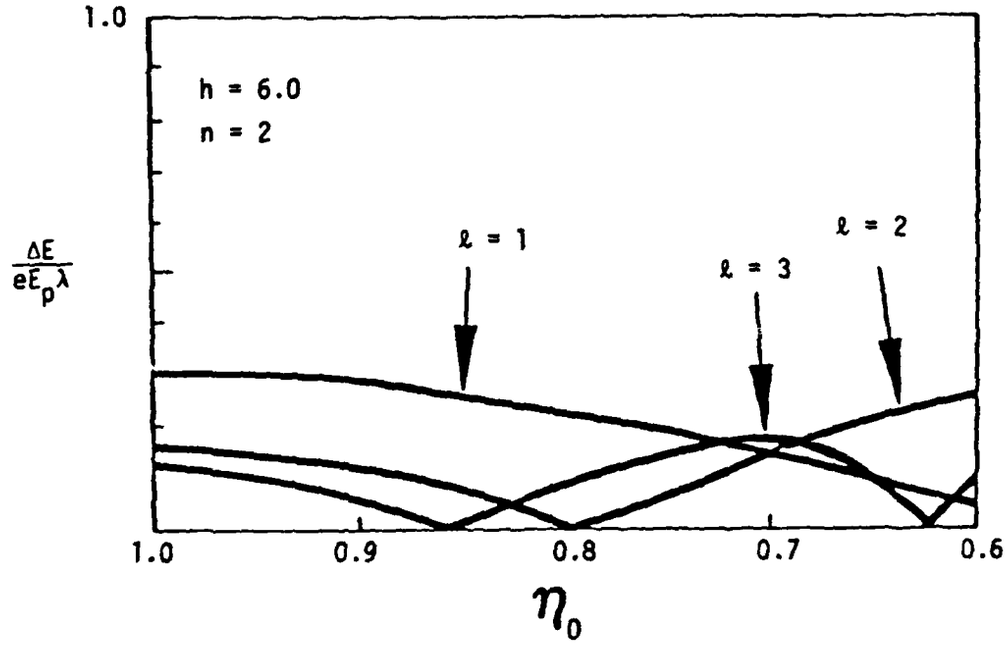

Figure 2. The coupling from RF fields to relativistic particles as function of the cavity opening for three radial modes and h = 6, n = 2.